This is the post-print. Formally published on 15-09-2025; Latest revised on 12-11-2025.

# 《量子物理与材料化学杂志》

## Journal of Quantum Physics and Materials Chemistry

ChengZhu Science™

江西省诚筑环保工程有限公司主办

Serials in September, 2025/2025 年第九月份期刊

出版人： 刘焕 香江出版社有限公司

**Publisher: Liu Huan, Xiangjiang Publishing Company Ltd.**




## Copyrights Statements

## Copying and Transferring is Forbidden!

## 版权申明

## 禁止复制、转载！

All the intellectual property (mainly including the original academic knowledges and brand logo) are prohibited to copy or transfer into other publications or websites. To cite this article, only short quote is acceptable, but copying or transferring any substantial part of this article is NOT allowed (Defined in <Copyright Ordinance> in Hong Kong). The original academic knowledge is the substantial part of an article as academic journal. For learning purpose, it is allowed to read our website in online video class only. This journal is published by Hong Kong Publisher, and the copyrights is regulated and protected by <Copyright Ordinance> in Hong Kong, China. This PDF document is accessible to public only through Hong Kong domain websites (natural-foundation-science.org), and its printed version is the formally published journal. Without permission, it is NOT allowed to print, issue and sale.

所有形式知识产权（主要包括原创型学术知识和品牌标识）禁止复制、转载到其他出版物和网站。如果需要引用这篇论文，仅仅允许简短引述，但是禁止复制、转载这篇论文中任何实质性部分（香港《版权条例》中定义）。作为学术杂志，这篇论文中的原创型学术知识即为作品的实质性部分。仅仅允许以学习为目的在线视频课堂阅读本公司网站。本杂志由香港出版社出版，其版权受中国香港《版权条例》监管和保护。此 PDF 文档仅仅通过香港主机网站向公众公开 (natural-foundation-science.org)，并且其印刷版本杂志为正式出版物。未经许可，不得印刷、发行、销售。

# Fundamental mechanics: from classical mechanics to quantum mechanics and its application on quantum chemistry

**DOI:**10.58473/JQPMC0014 Retrieval from: www.crossref.com

**Author:** Liu Huan (1983-), Master of Science (First Class Honours, 2009), The University of Auckland; Chief Editor, registered Editorial Board Memberships in Web of Science (Researcher ID: KCY-0721-2024).

**Formally published on 15/09/2025; Latest revised on 12/11/2025.**

**This research project is formally registered via Open Science Framework (OSF) Registry, with registration DOI:** https://doi.org/10.17605/OSF.IO/KRPC3

**Abstract/Study objectives:** it is first to conduct systematic review of mechanics theories, from Newton and his classical motion Laws, Einstein and his quantum mechanics, Black Body theory, wave-particle duality of De Broglie wave, photoelectric effect and Bohr atomic quantum model, finally to Schrodinger equation, based on which the new theories are proposed and discussed in detail in the first part; Then it is to select representative experiment research with regards to the above mechanics theories as case studies in this observation research project, and to further collect research data for re-editing into adapted version, which are re-analyzed on the basis of my newly proposed theories; Finally, it is to finish the artificial intelligence programs by C++ language, the 3D modeling of quantum chemistry proposed in my previous article.

**Key Words:** Classical Mechanics; Quantum Mechanics; De Broglie wave; Bohr Atomic Quantum Model; Schrodinger Equation; AI and Quantum Chemistry.

## Hypotheses

1.Why can these elementary particles (such as electron or proton) carry stable electric charges, whereas other elementary particles (such as neutron) carry little electric charges? If it can be explained, how they generate electric charges?

2.Does photon possess the attribute of mass? If it is, how to characterize the mass of photon? And how to input this variable of mass into the Mass-Energy formula?

3.Is the De Broglie wave of elementary particles significantly different from the classical materials wave? If it is, what is the difference between them in detail? And How to re-calculate the wave function of De Broglie wave for elementary particles?

## 1.Introduction of classical mechanics

First of all, it is to briefly introduce the milestones of classical mechanics in the science history that is outstandingly contributed by Newton. Then the applicable conditions and limitations of classical mechanics Laws are discussed to initiate the quantum mechanics chapter in modern science history.

### 1.1.Newton's First law of Motion

Any object's state remains in the forms of uniform motion or stationary state, until it is forced to change its state of motion, which is expressed as the equation:

$$\sum_i Fi = \frac{dv}{dt} = 0 \qquad \text{equation 1}$$

Fi is the composition of external forces, and $\frac{dv}{dt}$ is the accelerated velocity, representing that when the composition of external forces is zero, the accelerated velocity is zero, so the object's state remains in the forms of uniform motion or stationary state [24].

### 1.2.Newton's Second Law of Motion-Force and Acceleration

The acceleration of an object is positively relevant to the external force but negatively correlated to the mass of the object, with the same direction of acceleration as that of the resultant force, which is expressed as equation [25]:

$$F = m \times a \qquad \text{equation 2}$$

In this equation, a is the accelerated velocity.

### 1.3.Newton's Third Law of Motion-Force and Acceleration

Two interacting forces include both external force on object and the corresponding reaction force against the external force, so both are constantly equal in magnitude but opposite in direction acting on the same straight line, which is expressed as the equation [26]:

$$F = -F \qquad \text{equation 3}$$

### 1.4.Law of Universal Gravitation

In the universe, there is the force between any two objects to attract each other, called the universal gravitation, whose magnitude is proportional to the product of two objects' mass and inversely proportional to the square of their distance between them, with the expression equation [27]:

$$F = (G \times M_1 \times M_2)/R^2 \qquad \text{equation 4}$$

Where F represents the universal gravitation, G is the Gravitational constant ($6.67 \times 10^{-11}$ $N \cdot m^2/kg^2$), $M_1$ and $M_2$ are the mass of two objects, and R is the distance between both of them [27].

### 1.5.Limitations and pre-conditions of classical mechanics Laws

The classical mechanics Laws take effect that is subject to two hypotheses: firstly, it is assumed that the variables of both time and space are isolated (absolute) and the transmission of interaction between two objects is instantaneous, so the measurement of both spatial length and time interval is independent of the motion of the observer, which means that classical mechanics Laws actually apply only to situations under which the speed of object is much lower than the light. At high speeds, variables of both time and length can no longer be considered independent of the observer's motion; Secondly, all observable physics quantities can in principle be measured with infinite precision, which follows that classical mechanics Laws apply only to macroscopic objects, whereas in microscopic systems, it is in principle impossible to measure all physical quantities simultaneously. Therefore, the Laws of classical mechanics are the generally approximate equations suiting for the macroscopic objects of low-speed motion [28].

### 1.6.The mathematical application on vector of mechanics

Because the physical quantities of mechanics are usually the vectors, there are two common mathematical methods used to calculate the vectors' parameters in mechanics study, Lagrange method and Euler's method, both of which rely on partial derivatives and differential equations to resolve the component at each dimensional vector.

#### 1.6.1.Lagrange method

The spatial vector of r of a particle in space can be expressed as:

$$r = r(a,b,c,t) \qquad \text{equation 5}$$

In the Cartesian coordinate system (x, y, z), this vector formula is expressed as:

$$x = X(a,b,c,t) \quad y = Y(a,b,c,t) \quad z = Z(a,b,c,t) \qquad \text{equation 6}$$

When variables of a, b and c are fixed, the above equation represents the motion model in a specific spatial point; when t is fixed, it indicates the spatial distribution of all particles at the same moment. Therefore, the above equation describes the movement of all particles in three-dimensional space [29].

For a given spatial point, variables of a, b and c are constants, so if it is to find the rate of a physical quantity variation with respect to time, only the partial derivative of above equation need to be taken against 't' as [29]:

$$V = \frac{dr}{dt} = \frac{\partial r(a,b,c,t)}{\partial t} \qquad \text{equation 7}$$

$$u = \frac{\partial X(a,b,c,t)}{\partial t}\ , v = \frac{\partial Y(a,b,c,t)}{\partial t}\ , w = \frac{\partial Z(a,b,c,t)}{\partial y} \qquad \text{equation 8}$$

Where V is the speed of a particle in the spatial point (a,b,c), and variables of u, v and w are the component of vector 'r' at x, y, z axis respectively [29].

Similarly, the accelerated velocity can be derived by secondly taken the partial derivative against variable 't' as [29]:

$$a = \partial^2 r(a,b,c,t)/\partial t^2 \qquad \text{equation 9}$$
$$a_x = \partial^2 X(a,b,c,t)/\partial t^2$$
$$a_y = \partial^2 Y(a,b,c,t)/\partial t^2$$
$$a_z = \partial^2 Z(a,b,c,t)/\partial t^2$$

Where variables of a, $a_x$, $a_y$, $a_z$, are the accelerated velocity, and its component at x, y, z axis, respectively [29].

### 1.6.2. Euler's method

Euler's method is another common method used to resolve the vector of wave function in mechanics study, which will be in detail illustrated in the following wave function sections. In Euler's method, the Operator of formula is adopted to simplify the calculation process.

## 2.Einstein and his quantum mechanics

### 2.1.Study objective of quantum mechanics

Matter in nature exists at multiple scales, spanning from the vast cosmic space, macroscopic celestial bodies, conventional objects, tiny particles, fibers, crystals, to the microscopic scale of molecules, atoms, and elementary particles. Forms of mechanics motion encompass movement, rotation, flow, deformation, vibration, fluctuation, diffusion, among which the balance and stillness status is the special state of motion. Mechanical motion stands as the most fundamental form of material motion, while other forms of material motion include thermal motion, electromagnetic motion, atomic and internal motion, as well as chemical motion, but mechanical motion usually co-exists with other forms of motion [14].

Photon that was also defined as light quantum referred to a kind of elementary particle transmitting electromagnetic interactions, which was a gauge boson proposed by Einstein in 1905 and was subsequently officially named by an American physical chemist, Gilbert Lewis, in 1926. It was proposed that photons were the carriers of electromagnetic radiation and in theory of quantum physics, photons were considered as mediators of electromagnetic interactions. The static mass of photons was deemed to be zero, and photons moved at the speed of light, which possessed the properties of energy, momentum and mass [15].

Particularly, modern quantum mechanics has introduced the conceptional model of high-dimensional spaces into its theoretical demonstration, not limiting to three-dimensional spaces, such as Time-Space proposed by Einstein who argues that the fourth dimensional space is defined as the inertial system along time axis, and M-theory proposed by Hawkin who classifies the high dimensional spaces into 11 dimensions in the universe. However, my another article has newly modified and redefined the conceptions of high dimensions in quantum mechanics theory [8].

## 2.2.Attributes of photons

When Einstein pointed out that in addition to energy ε, photons must also be characterized by using the attribute of impulse, the direction of which corresponded to the direction of light propagation, in order to improve the interpretation of photons. According to his theory of special relativity, compared with most elementary particles, photons possessed zero mass in static, which meant that their propagation speed in vacuum was the speed of light. Like other quanta, photons showed wave particle duality: photons could exhibit wave properties, such as refraction, interference, diffraction and etc. like classical mechanics waves, while the particle nature of photons could be demonstrated by the photoelectric effect. Photons could only transmit quantized energy, so they were space-lattice particles [15].

After the establishment of the theory in quantum electrodynamics, it was confirmed that photons were the medium particles for transmitting electromagnetic interactions, so charged particles interacted each other by emitting or absorbing photons, and both positively and negatively charged particles could be annihilated, converting into photons, which could be generated in electromagnetic fields. More specifically, a pair of both positive and negative particles could annihilate into a pair of high-energy γ photons, while a pair of high-energy γ photons could also react at high temperature to generate a pair of positive and negative particles correspondingly. For example, the conversion of photons into baryons, such as protons and neutrons, could occur at high temperature T = 1015k. The positron - negative electron scattering, which was also named as Bha-Bha scattering, was interpreted by Feynman diagram, whose wave line represented the process of exchanging virtual photons [15].

Defined by the special relativity, photons were the particles in light that carried energy, which was proportional to the frequency of the light wave, so the higher the frequency, the higher the energy. When a photon was absorbed by an atom, an electron gained enough energy to transition from the inner orbit to the outer orbit, turning the atom from the ground state to the excited state [15].

## 2.3.Mass-Energy Equation

According to Einstein's special relativity, the physical attributes could be converted into each other among photons' energy, momentum and mass. On the basis of the mass-energy equation,

$$E = mc^2 = h\nu \qquad \text{equation 10}$$

Then the mass of photons could be calculated into: $m = h\nu/c^2$, where parameters of h,ν and c were the Planck constant, frequency of light wave, light speed constant respectively, and particularly this mass was defined as the relative mass only without static nature [15].

Due to the differentiation of static mass from motion mass, there is the conception of 'deficit conservation' proposed: when a cluster of particles aggregates to form a composite object, due to the existence of interaction energy between the particles and the kinetic energy based on the relative motion, the aggregated object as a whole is stationary, whose total energy is generally not equal to the sum of the stationary energies of all particles. Consequently, the difference between these two is expressed as mass-energy inequation below [16]:

$$E_0 \neq \sum Mi_0 \times c^2 \qquad \text{equation 11}$$

where $Mi_0$ is the stationary mass of each elementary particle and is the total energy of aggregated object. According to the mass-energy equation, it is deduced that the difference between the two is attributed to the binding energy among the elementary particles of the aggregated object, which can be calculated as [16]:

$$\Delta E = \sum Mi_0 \times c^2 - E_0 \qquad \text{equation 12}$$

Where ΔE is represented as the binding energy of the aggregated object. Correspondingly, the static mass of an aggregated object is not equal to the sum of the static mass among the elementary particles that make up it, whose difference between the two is called mass loss (ΔM), calculated as [16]:

$$\Delta M = \sum Mi_0 - M_0 \qquad \text{equation 13}$$

Where $M_0$ is the static mass of aggregated object. It is further deduced that there is the relationship between static mass loss and binding energy [16]:

$$\Delta E = \Delta M \times c^2 \qquad \text{equation 14}$$

## 2.4.Energy - Momentum equation

In vacuum, the velocity of photons was identical to the velocity of light, with the relationship between energy E and momentum P as: $P = E/c$, under the hypothesis of zero static mass. It was further deduced that both energy and momentum of photons were only related to the frequency ν of light wave (or it was only related to the wavelength λ of light wave), so the momentum of photon could be also calculated as [15]:

$$P = h/\lambda = h\nu/c \qquad \text{equation 15}$$

in comparison, for other elementary particles with static mass above zero in relativistic mechanics, the energy-momentum (E-P) relationship of a elementary particle with static mass ($m_0$) was calculated as [15]:

$$E^2 = (Pc)^2 + (m_0c^2)^2 \qquad \text{equation 16}$$

**2.5.Explanation and modification of Einstein's special relativity**

However, another viewpoint disagreed with the meaning of the mass-energy equation above, which argued that the mass-energy equation did not reveal the conversion relationship between mass and energy, but the mass - energy equation only reflected the relationship between mass and energy in quantity. For a closed system in which mass was conserved and energy was also conserved, when the existing form of matter changed, the form of energy also changed correspondingly, but the mass was not converted into energy in the process of material reaction and conversion, so both mass and energy represented the properties of matter: mass property described inertia and gravitation, while energy property described the state of the system [16].

The mass-energy equation described the relationship between mass and energy, so it did not violate the law of conservation of mass. The formula showed that matter could be transformed into radiant energy, at the same time radiant energy could also be transformed into matter, which did not mean that matter would be eliminated, but the static mass of matter would be converted into another motion form [16].

Einstein firstly proposed that the formula showed that an object still possessed energy when it was stationary relative to a reference frame, which was contrary to Newton's system, because in Newton's system, a stationary object was deemed as zero-energy, which became the reason why the mass of an object was called a stationary mass. The variable of E in the formula could be regarded as the total energy of the object, which was proportional to the total mass of the object, including both static mass and mass in motion. Only when the object was stationary, it became proportional to the static mass of the object that was consistent with the 'mass' definition in Newton's system. He also argued that the total mass of the object was different from the static mass, by illustrating that a beam of photons propagating in a vacuum was deemed to possess zero static mass, but they showed motion energy, so they also had mass [16].

It was further explained that the static energy of an object was identical to its total internal energy, including the kinetic energy of molecular motion, the potential energy of inter-molecular interaction, the chemical energy that combined atoms with atoms, the electromagnetic energy that combined nuclei with electrons in atoms, and the binding energy connecting protons and neutrons in nuclei. The revelation of the static energy of matter was considered as one of the most important corollaries of relativity, which pointed out that there was still motion inside a static particle that had certain

internal motion energy with certain mass; in turn, a particle with certain internal motion energy showed certain inertial mass correspondingly. In the process of elementary particle transformation, it was possible to release all the static energy contained in the particle, turning it into usable kinetic energy. For example, when a π meson decays into two photons, the static mass of the photons is zero and static energy disappears, so the π meson contains all the static energy of matter before it decays [16].

In summary, this mass-energy equation critically contributes to the development of the atomic bomb. By measuring the mass difference between the mass of nuclei and the sum mass of both independent protons and neutrons at the corresponding quantity, it is to obtain the estimated value of the binding energy contained in the nucleus, which does not only show the phenomenon that the nuclear binding energy may be released through both nuclear fusion (for lighter nuclei) and nuclear fission (for heavier nuclei), but also can be used to quantitatively estimate the amount of binding energy that will be released. It is worthwhile noting that the masses of both protons and neutrons do not disappear over the nuclear reaction process, whose mass also represents the energy value. This equation stems from Albert Einstein's study with regards to the relationship between the inertia of an object and its own energy. The famous conclusion of his study is that the mass of an object is actually to measure its internal energy. In order to better understand the importance of this relationship, it is to compare electromagnetic force with gravity force. According to the theory of electromagnetism, energy exists in both electric field and magnetic field that is related to force but independent of electric charges, whereas in the theory of universal gravitation, energy is contained in matter itself. Therefore, it is concluded that the mass of matter can distort space-time in his special relativity, but the other three basic interactions among elementary particles, including electromagnetic interaction, strong interaction and weak interaction, cannot achieve the space-time distortion [16].

### 2.6.Critical discussion of quantum mechanics

It is to further clarify some conceptions originally proposed in my previous articles:

#### 2.6.1.Elementary particles and electric charge generation

In my previous article [10], it has been proposed that the magnetic line on the fourth dimension axis is perpendicular to the three-dimensional space and these magnetic elementary particles cut along the magnetic line on the fourth dimensional axis, thus generating electric charges. My another article has proposed that “in our three-dimension space, the protons are positively charged and the electrons are negatively charged; the materials in correspondingly symmetric three-dimensional space along the fourth dimension axis is called antimatter, in which the protons are negatively charged and the electrons are positively charged [3].” Consequently, the magnetic line that is perpendicular to our three-dimensional space is definitely the magnetic line connecting both symmetric three-dimensional spaces, and the elementary particle motion cutting along this perpendicular magnetic line is the

spinning motion of elementary particle by itself. It can be easily deduced that the directions of spinning motion are opposite between protons and electrons along this perpendicular magnetic line connecting both symmetric three-dimensional spaces, so that their electric charges are positive and negative correspondingly.

My quantum physics article has defined that "quantum photon is the mass particle that is coated and surrounded by dark matter in the fourth dimension, so that its static mass can be hardly detected by particle collider instrument, but this particle must be the mass carrier for quantum energy." It is further proposed that photons generate electromagnetic waves by the wave-like transmitting movement inside the dark matter, and this wave-like transmitting movement cuts the magnetic line along the fourth dimension axis that is parallel to the sphere surface of our three-dimensional space (different from the perpendicular magnetic line connecting both symmetric three-dimensional spaces). Electromagnetic waves are the energy form matter existing only as electric field and magnetic field. However, if the electromagnetic wave of energy form leaves the the carrier of photons, it can be easily absorbed by other materials (including dark matter) in this universe.

It is clarified that there are two kinds of the fourth dimensional axes defined in my journal: one is the axis along the magnetic line that is perpendicular to our three-dimensional space and connects two symmetric three-dimensional spaces, and the other one is the axis along the magnetic line that is parallel to the sphere surface of our three-dimensional space, as my previous articles [17][18] have demonstrated that the three-dimensional space where we are living is the curved sphere. My electromagnetism article has discussed the parallel space that "the propagation directions of the electric field and the magnetic field are parallel and opposite in the fourth dimension axis, but in the corresponding three-dimensional space, they turn to be the mutually vertical propagation directions due to the refraction effect [2]," and this magnetic line in the fourth dimension axis refers to the first magnetic line that is perpendicular to our three-dimensional space and connects two symmetric three-dimensional spaces. In summary, the generation of electric charges by the spinning motion of elementary particles in atom, the generating of electromagnetic wave by the wave-like transmitting movement of photons, and the change of magnetic line propagation direction due to the refraction effect at the sphere surface of our three-dimensional space are further demonstrated in Figure 1, Figure 2 and Figure 3, respectively.

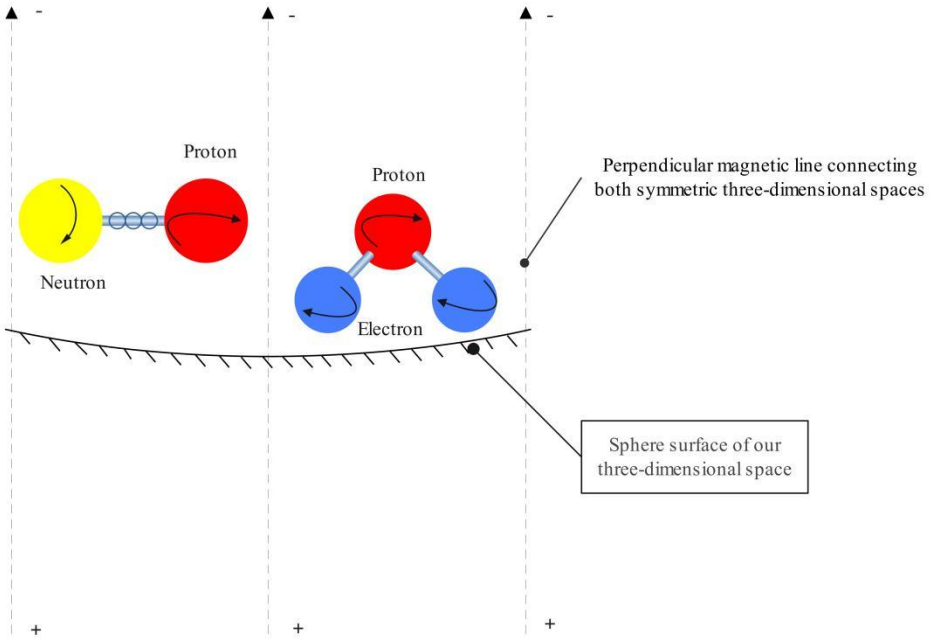



**Figure 1. The generation of electric charges by elementary particles in atom.**

Figure 1 illustrates the spinning motion of elementary particles in atom, generating electric charges. In this conceptional model, it is hypothesized that protons spin from left to right direction, while electrons spin from right to left, and both proton and electron's spinning motion cuts the perpendicular magnetic line connecting both symmetric three-dimensional spaces, thus generating positive and negative charges respectively. In comparison, neutrons spin from up to down, whose spinning motion direction is parallel to the perpendicular magnetic line connecting both symmetric three-dimensional spaces, consequently generating little electric charges.

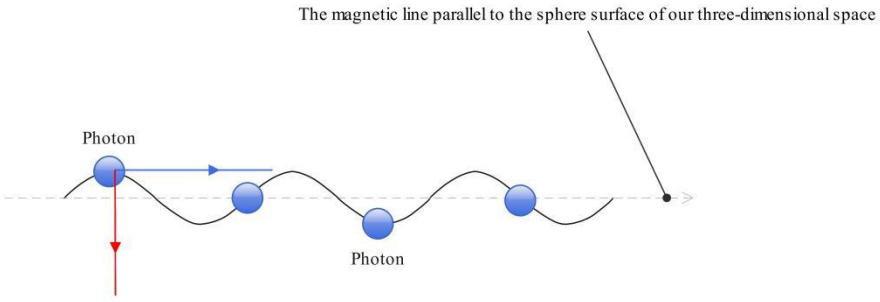



**Figure 2. The generating of electromagnetic wave by photons.**

Figure 2 illustrates the generation of electromagnetic wave by the wave-like transmitting movement of photons in dark matter. The wave-like movement of photon can be divided into two sub-vectors: one is the transmitting movement (indicated by

the blue arrow) along the magnetic line that is parallel to the sphere surface of our three-dimensional space, releasing magnetic field energy, and the other one is the cutting movement (indicated by the red arrow) against this magnetic line, releasing electric field energy. Consequently, this motion model also reveals both magnetic and electric energy distribution characteristics of electromagnetic wave in three-dimension space.

Further more, when the elementary particles decay, it displays as the spring-like shaking movement, whose direction is vertical to the sphere surface of our three-dimensional space (in Figure 1), thus generating longitudinal wave (such as rays); in comparison, the electromagnetic wave generated by the wave-like transmitting movement of photons in dark matter is the transverse wave.

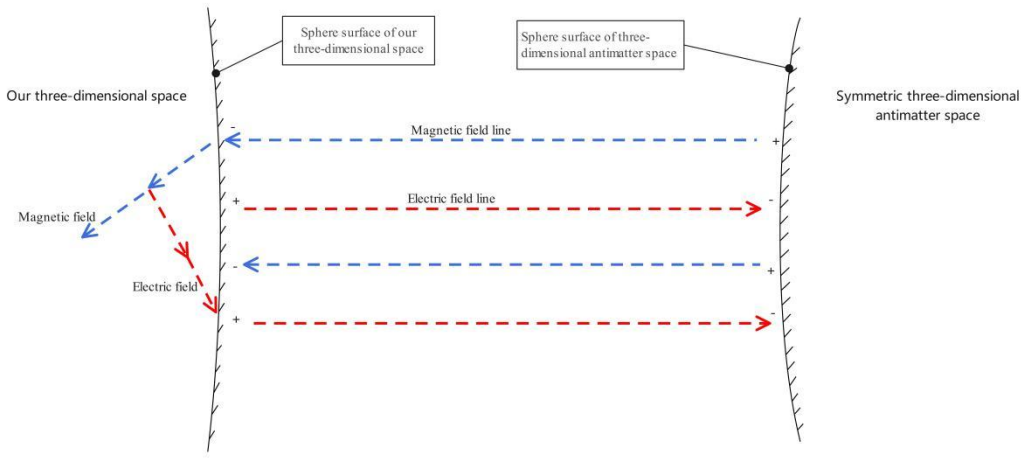



**Figure 3. The propagation direction of both magnetic line and electric line between two symmetric three-dimensional spaces.**

In Figure 3, there are two symmetric three-dimensional spaces outlined (our three-dimensional space is on the left and the symmetric three-dimensional antimatter space is on the right in Figure 3). Between both symmetric three-dimensional spaces, the space is defined as the 'parallel space', in which the propagation directions of the electric field and the magnetic field are parallel and opposite (the red line indicates electric field line and the blue line indicates magnetic field line). In our three-dimensional space, the propagation directions of magnetic line and electric line become mutually vertical, but the refraction effect at the sphere surface of our three-dimensional space leads both to change the propagation directions as shown in Figure 3.

### 2.6.2.Mass-Energy equation

My article agrees with Einstein's special relativity which firstly argues that mass can be converted into energy, disagreeing with the 'energy/mass conservation Law.' It is further proposed that nuclear fusion reaction converts the mass of elementary particles into energy, while nuclear fission reaction converts the mass of dark matter into

energy that is also the indicator of binding energy among elementary particles. Consequently, the mass of matter, including dark matter and elementary particles, is regarded as a kind of the form for energy storage.

### 2.6.3.The energy-momentum equation of elementary particle

Figure 2 has divided the movement of photon into two sub-vectors, indicated by the blue arrow and red arrow respectively, so the momentum of photon is correspondingly divided into two kinds of vector momentum as well. It can be deduced that the cycle of the wave-like mechanical movement of photon (shown in Figure 2) determines the frequency (ν) of the correspondingly generated electromagnetic waves, so the relationship between momentum of photons and energy can be further modified into: the electric energy ($E_e$) is positively correlated with its corresponding momentum (indicated by the red arrow) of photon and is negatively correlated with the wavelength (λ) of the wave-like mechanical movement (or positively correlated with the frequency of the wave-like mechanical movement). Consequently, the vector momentum of photon (indicated by the red arrow) can be calculated into:

$$P1 = a \times E_e / \lambda \qquad \text{equation 17}$$

where the variable P1 and parameter a is the vector momentum of photon (indicated by the red arrow) and its corresponding constant, respectively; the magnetic energy ($E_m$) is positively correlated with the light speed (c) and its corresponding momentum (indicated by the blue arrow), so the vector momentum of photon (indicated by the blue arrow) is calculated as:

$$P2 = b \times E_m \times c \qquad \text{equation 18}$$

where the variable P2 and parameter b is the vector momentum of photon (indicated by the blue arrow) and its corresponding constant, respectively. Obviously, the variables of both $E_e$ and $E_m$ of light waves can be feasibly measured in experiment, so that variables of both P1 and P2, together with constant a and b, can be correspondingly estimated according to the regression analysis.

In my quantum mechanics article, it is argued that “when two beams of charged particle collide in the particle collider, under the condition that the law of electromagnetic induction can be ignored, the kinetic mechanics of a beam of charged micro-particles only conforms to the principle of fluid mechanics (such as pressure calculations), and is not applicable on the mechanical energy law of solid collision (such as conservation of momentum).[1]” My article further proposes that the beams of charged elementary particles in the particle collider and the emitted charged elementary particles during the atom decaying process also show the wave-like mechanical movement over the transmitting process due to the nature of dark-matter, which is similar to photon’s movement shown in Figure 2, but their static mass can be detected in experiment, because their aggregated masses display in our

three-dimensional space. However, the static mass of elementary particles is not constant in our three-dimensional space, as my quantum mechanics article has proposed that "These elementary micro-particles randomly fluctuate along the fourth dimension axis, so the mass of micro-particles in the three dimensions space isn't constant.[1]" Hence Figure 4 of this article has further illustrated this movement model of the beams of charged elementary particles in the particle collider in more details.

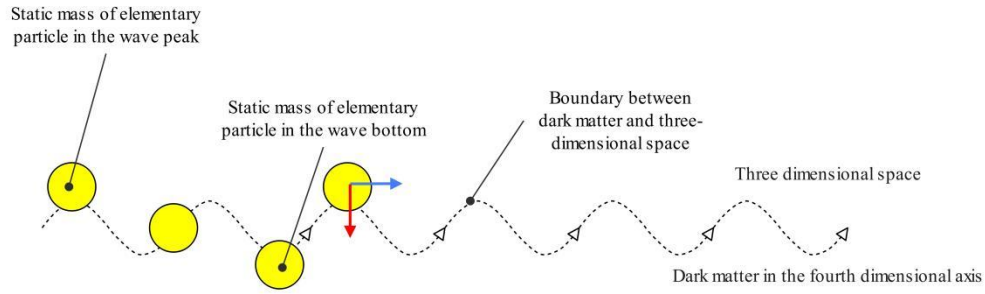



Figure 4. The mass of elementary particle in the acceleration motion process inside particle collider.

As shown in Figure 4, the movement model of a beam of charged elementary particles in the particle collider instrument displays as the wave-like transmitting motion due to the nature of dark matter. The boundary between the dark matter of the fourth dimensional axis and our three-dimensional space becomes the line partitioning the static mass that displays in our three dimensional space and can be consequently measurable by using equipment. At the wave peak, the static mass displaying in our three dimensional space is the highest, then decreasing with the transmitting direction, and shows the smallest at the wave bottom position. Consequently, the static mass of elementary particles that display in our three-dimensional space varies with the wave-like transmitting motion, so the energy-momentum (E-P) equation for elementary particles with static mass is further modified into:

$$E^2 = \alpha\times(P\times v)^2 + (m_0\times c^2)^2 \qquad \text{equation 19}$$

In this equation, the part of $\alpha\times(P\times v)^2$ represents the energy generated by the vector motion (indicated by the red arrow) that is vertical to the boundary between dark matter and three-dimensional space, in which the parameter $\alpha$ is the constant; the equation part of $(m_0\times c^2)^2$ represents the energy generated by the vector motion (indicated by the blue arrow) that is parallel to the particle acceleration motion direction, in which the variable $m_0$ is the static mass of elementary particles, and the variable c is the acceleration motion speed.

## 3. Black body

### 3.1.Blackbody radiation and absorption

An ‘absolute blackbody’ is a theoretical model that refers to an object absorbing all light at any wavelengths without any reflection. Once a beam of light wave penetrates into a cavity through a slit hole, it is difficult for the light wave to pass through the same slit hole in the opposite direction, and the opening of this cavity can be considered a blackbody (Figure 5 (left)). In theory all objects in the world are constantly absorbing and emitting infrared radiation, and a blackbody is considered as the ideal emitter and absorber of infrared radiation in this theory. For example, black holes are the typically idealized absolute blackbodies, which absorb the infrared waves of all wavelengths [19].

Experiments have shown that under the condition that a blackbody reaches equilibrium with thermal radiation, the radiation energy density (Er) is only related to the thermodynamic temperature (T) of the blackbody, which is independent of the shape and composition of the cavity[19]. In the radiation spectral line of blackbodies, the color of light varies with the temperature ascending, which exhibits the order of transition from red → orange red → yellow → yellow white → white → blue white. When the color of a light source is adjusted to be the same as the color of light that is emitted by a blackbody at a certain temperature (T), then this critical temperature of the blackbody is called the color temperature of the light source. The higher the temperature of a blackbody, the more blue light wave components contained in its spectrum, while the less red light wave component is emitted from the light source. For example, the color of incandescent lamps is warm white, with a color temperature of 2700K, while the color temperature of daylight fluorescent lamps is 6000K, emitting fluorescent light waves [20].

Kirchhoff Radiation Law hypothesizes that under thermal equilibrium, the ratio of the energy radiated by an object to the absorptivity is irrelevant with the physical properties of the object itself, but is only related with wavelength and temperature. According to Kirchhoff Radiation Law, at a certain temperature, a blackbody must be the object with the greatest radiation capacity, consequently called as the complete radiator, which means that blackbody radiation reaches the maximum amount of emission at a specific temperature and wavelength. At the same time, blackbody is an object that can absorb all incident radiation and will not reflect any radiation, the colour of which is not necessarily black. For example, the sun is a gaseous planet, which can be considered that the electromagnetic radiation emitted to the sun is difficult to be reflected back, so the sun is considered that the sun is a blackbody, although the absolute blackbody does not really exist. Theoretically, blackbody does not only absorbs electromagnetic waves of all wavelengths in the spectrum, but also emits electromagnetic waves of all wavelengths in the spectrum. Wien’s displacement law describes the relationship between the peak wavelength of the electromagnetic radiation energy flux density and the temperature of blackbody, which is further developed by Planck [20].

Planck hypothesis: there are charged linear harmonic oscillators in the radiation

material, and these harmonic oscillators can only exist under certain States. Under these States, the corresponding energy is the integral multiple of the minimum energy ε that is defined as energy quantum, so the radiation energy is expressed as: ε, 2ε, 3ε, nε,..., among which n is a positive integer. According to this hypothesis, the famous Planck blackbody radiation formula is derived:

$$\rho(v,T) = \frac{8\pi hc}{\lambda^2} \times \frac{1}{e^{hC/\lambda kT} - 1} \qquad \text{equation 20}$$

Where ρ is the radiation energy density, v is the frequency of harmonic oscillators, T is the temperature, h is the Planck constant, λ is the wavelength, c is the light speed, and k is the Boltzmann constant. In this Planck blackbody radiation formula, the radiation energy density is the function of variable v and T, which is the improved formula of Stefan-Boltzmann formula.

### 3.2. Original discussion of blackbody radiation and absorption

My article has firstly proposed that "According to the Figure 1 of my article [11], it is to further discuss the argument of the shielding effect of the electric field inside an atom and its effects on the electron orbitals; Multiple equipotential lines are formed between the zones of constructive interference and the zones of destructive interference." Consequently, it is here to argue that the shielding effect of the equipotential field lines inside an atom or a molecule causes the phenomenon of 'blackbody' radiation and absorption described above.

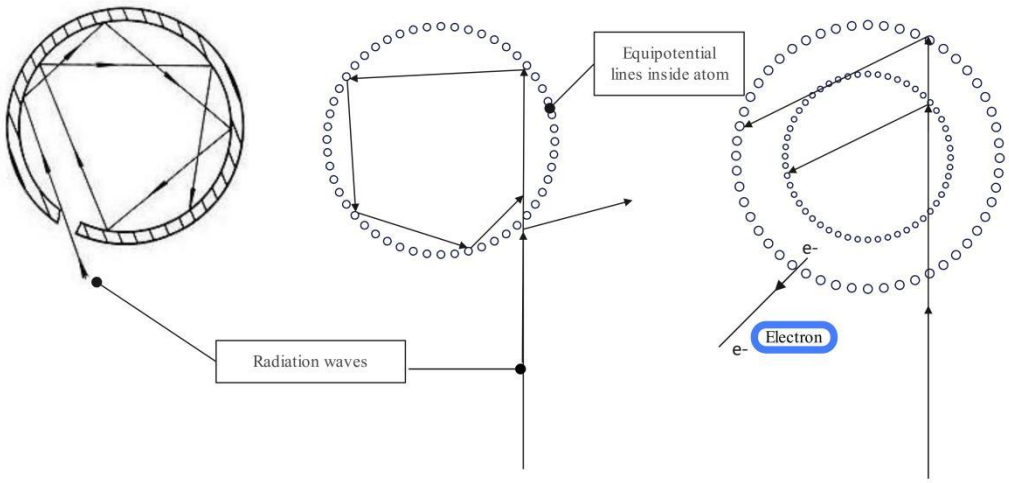



Figure 5. Blackbody radiation and absorption mechanism.

As can be seen from Figure 5 (left), the structure of sphere 'shell' and the slit hole on the shell explains the old 'blackbody' formation theory, but my new theory proposes that the equipotential field lines inside an atom or a molecule play the role in the shielding effect instead of the 'shell' of 'blackbody'. After the radiation waves have

penetrated into the equipotential field lines, this shielding effect does not only stop the radiation waves from releasing out of the atom, but also causes a small proportion of radiation waves that reflect on the surface of the shielding lines, shown in Figure 5 (middle). Consequently, an 'absolute blackbody' does not really exist. When the temperature ascends, free electron shifts from inner atomic orbital to the outer orbital, so that the equipotential field line causing shielding effects is shifted correspondingly (shown in Figure 5 (right)), which results in the variation of 'blackbody' radiation waves, expressed as different color temperature discussed above.

It is further concluded that the shielding effects of the equipotential field line inside an atom or molecule plays the important role in the conserving the energy of an atom or molecule, and keeping the stable structure of elementary particles, whose mechanism is similar to the 'blackbody' theory.

## 4.Wave particle duality of substance waves

### 4.1.From classical wave to De Broglie wave

De Broglie wave, also named as the material wave, is a kind of wave expressing spatial probability in microscopic particle occurrence, which refers to the probability that may occur in a specific spacial point at transient time, and this particle occurrence probability is controlled by the fluctuation law. Mechanical wave is the propagation of periodic vibration in the medium, and electromagnetic wave is the propagation of periodic electromagnetic field, whereas material wave is neither mechanical wave nor electromagnetic wave [21]. Thus the material wave is proposed to explain the light wave at quantum level, which can be hardly deduced by the classical mechanical wave or electromagnetic wave theories.

Davidson and Dermot emitted single energy electron onto the polished plane of nickel single crystal, aiming to observe the quantitative relationship between the intensity of scattered electron beam and scattering angle. Both emitting source of electron beam and the scattered electron detector were symmetrically placed on the normal of the crystal surface, and the experiment showed that the intensity of the scattered electron beam varied with the scattering angle (θ). When the scattering angle was adjusted to be a critical value, the scattering intensity reached the maximum value, which was the same as the phenomenon of X-ray diffraction, fully proving that the electron had wave particle duality. Because the electrons with low energy (in Davidson's experiment, the electron energy was set to be about 30~400 ev), which could not penetrate deeply into the crystal, most of the electrons were scattered on the crystal surface [19].

According to the diffraction theory, the position of the maximum diffraction value is determined by the following formula [19]:

$$n\lambda = 2d\times\cos(0.5\theta) \qquad n = 1, 2, ... \qquad \text{equation 21}$$

Where n is the order of diffraction maximum, λ is the wavelength of the diffractive ray, and d is the crystal plane spacing of crystal Bragg scattering. Setting up parameter of d (the crystal plane spacing of nickel single crystal) = 0.091nm, when the electron beam energy is 54 ev and the scattering angle (θ) is 50°, respectively, a maximum diffraction peak is observed. According to the Bragg equation, the electron wavelength can be calculated to be 0.165 nm [19].

There is the parallel calculation according to the de Broglie relation, the wavelength of the electron can be also calculated in another way [19]:

$$\lambda = \frac{h}{p} = \frac{2\pi\hbar c}{\sqrt{2m_e c^2 E}} \qquad \text{equation 22}$$

In this equation, λ is the wavelength, c is the electron speed, h is the Planck constant, P is the electron momentum, ħ is the reduced Planck constant, ħ = h/2 π, $m_e$ is the electron mass, and E is the kinetic energy of electron. Many experiments have shown that, in addition to electrons, all the other microscopic particles at various sizes, such as neutrons, protons, mesons, atoms, molecules and even C60 molecules, also display as the wave motion, so de Broglie formula is also applicable on these particles. Therefore, de Broglie formula is a basic formula to express the wave particle duality of various microscopic particles [19].

### 4.2.The wavelength of electron de Broglie wave

Under the conditions that the kinetic energy of a free particle is E, the momentum is p, and the particle velocity is much lower than the speed of light, then the de Broglie wavelength of electron's material wave is calculated as [19]:

$$\lambda = \frac{h}{p} = \frac{h}{\sqrt{2\mu E}} \qquad \text{equation 23}$$

Where $\mu$ is the electron mass. If an electron is accelerated under the electric field with the potential difference of U in a transmission electron microscope, and usually the acceleration voltage of an electron microscope is 200~300 kV, then the electron kinetic energy is calculated as: E = eU, among which e is the electron charges, so the de Broglie wavelength of electron's material wave is further estimated as [19]:

$$\lambda \approx \frac{12.25}{\sqrt{U}} \text{ (Å)} \qquad \text{equation 24}$$

After determining the specific values of parameter h, μ, and e, the de Broglie wavelength of electron's substance wave is estimated as: when U = 150 kV, λ = 1Å $=10^{-10}$ m; when U = 10000V, λ = 0.122 Å. It can be seen that the wavelength of the de Broglie wave of electrons is very short, whose order of magnitude is equivalent to the atomic spacing in crystals, much shorter than macroscopic linearity of mechanical

wave. Therefore, the wave particle duality of physical particles, which is derived empirically under general macroscopic conditions, will not be applicable on the microscale any more (particle nature is the main contradiction aspect), so a new mechanics - quantum wave dynamics - must be established to cope with the quantum level material wave [19].

### 4.3.The substance plane wave

In classical mechanics, if the angular frequency is ω and the wavelength is λ, the propagation motion of substance plane wave along the x-axis direction can be expressed as [19]:

$$\psi(x,t) = A\times\cos(k\cdot x - \omega\cdot t) \qquad \text{equation 25}$$

Where the wave vector of $k = 2\pi/\lambda$; the constant A is the wave amplitude; t is the propagation time [19].

For the convenience of calculation, it is to transform the above wave function by integrating the Euler formula: $e^{ix} = \cos(x) + i\times\sin(x)$, among which parameter i is the imaginary unit. Then the substance plane wave function can be expressed as [19]:

$$\psi(x,t) = A\times\exp[i\times(k\cdot x-\omega t)] \qquad \text{equation 26}$$

This wave function is used to describe the X-rays motion that displays as Bragg diffraction phenomenon. Since microscopic particles such as free electrons are also capable of showing diffraction stripes similar to X-rays, the de Broglie wave of free microscopic particles can also be described by this wave function. By inputting the above equations, $E = h\nu$ and $\lambda = h/p$, into this classical mechanics function, the free particle plane wave function is expressed as [19]:

$$\psi(x,t) = A\times\exp[\tfrac{i}{\hbar}\times(p\cdot x-E\cdot t)] \qquad \text{equation 27}$$

This is the function describing the substance plane wave associated with free microscopic particles, the transformed equation of de Broglie wave, which is derived from the classical macroscopic wave function. It describes the motion state of free particle by integrating momentum p and energy E, which is the de Broglie wave specifically describing the free microscopic particles. If the particle motion trajectory varies both spatially and temporally under the potential field, its momentum and energy are no longer constant (or both physical variables are not constant concurrently), and then the particle is no longer in the form of free particle, so its motion model cannot be described by the plane wave derived from the classical macroscopic wave function. Instead, as the particle still possesses the attribute of wave particle duality, it must be described by more complex wave function (e.g., Bloch wave function describing the electron wave motion in solids) [19].

### 4.4.Photoelectric effect

It is observed that when ultraviolet light or visible light at short-wavelength hits the metal in vacuum, electrons will escape from the metal surface, so this observed phenomenon is called photoelectric effect, and the escaped electron is called photo-electron, whose experiment has resulted in the conclusions below [19]:

Firstly, in the same period, the number of photo-electrons released from the radiated metal surface is proportional to the intensity of the incident light; Secondly, the initial kinetic energy of the photo-electron increases linearly with the frequency of the incident light (ν), regardless of the intensity of the incident light, which means that the intensity of incident light does not influence the kinetic energy of the photo-electrons; Thirdly, when the incident light radiates onto a specific type of metal, there is no photoelectric effect occurring, if the frequency of incident light is less than the critical frequency limit ($\nu_0$) of the specific metal, regardless of the intensity of the light, which means that there is the threshold of incident light frequency for a specific type of metal to generate photoelectric effect; Fourthly, when the incident light frequency exceeds the threshold frequency ($\nu_0$), the photo-electrons are capable of being observed almost immediately as long as the light shines on it (about 10-9s after the incident light hits the metal), no matter how weak the incident light intensity is [19].

Firstly, it is to try to explain the photoelectric effect experiment results according to the classical electromagnetic theory of light as: when the light shines onto the metal surface, the electrons in the metal are forced to vibrate by the electric field of the incident light, which causes to absorb the energy from the incident light and hence escape from the surface, so the amount of the obtained energy should be related to the intensity of the incident light and the period of the light radiation, but is independent of the frequency. According to this classical mechanics wave theory, as long as there is sufficient light intensity or sufficient irradiation time, there is always a photoelectric effect for any incident light frequencies, whose conclusions are all in direct contradiction to the experimental results. Consequently, these conclusions of the photoelectric effect are incapable of being explained by the classical mechanics wave theory [19].

### 4.5. Bohr atomic quantum model

The wavelength of light source can be derived from hydrogen atomic spectroscopy:

$$\lambda = B\times\frac{n^2}{n^2-4}\ , \qquad \text{equation 28}$$

where B is a constant, and its estimated value is $B = 3.645610^{-7}$m; n=3,4,5,... [19].

This wavelength equation is extended to the general formula[19]:

$\tilde{\nu} = k_R \times (\frac{1}{K^2} - \frac{1}{n^2})$, (where $k_R$ is Rydberg constant, K = 2,3,4,...; n>k) equation 29

In this equation, $\tilde{\nu}$ is the wave number ($\tilde{\nu} = 2\pi/\lambda$), and thus the conclusions of the hydrogen atomic spectrum are drawn as: the wavelength is determined by the difference between the two spectral items ($\frac{1}{K^2}$ and $\frac{1}{n^2}$); if the K value of first spectral item ($\frac{1}{K^2}$) is fixed and the n value of the second item ($\frac{1}{n^2}$) is given by different values, the wave number of each spectral line in the same spectrum is obtained; if it is to change the k value of the first term, then different spectrums can be obtained [19].

$$\text{Rydberg constant } k_{\tilde{\nu}} = \frac{\mu e_s^4}{4\pi h^3 c} \qquad \text{equation 30}$$

The specific values of parameter μ, e, $\varepsilon_0$, c and h are input into the above formula, and the R value accurately agrees with the values measured by the experiments [19].

However, these conclusions derived from the hydrogen atomic spectrum experiment are unexplained by the classical electrodynamics theories. Firstly, the classical theory cannot establish a stable atomic model to explain the continuous rotation motion of electrons around the nucleus. According to the classical electrodynamics, the movement of electrons around the nucleus is accelerated, generating the continuous radiation of electromagnetic waves, which results in continuous loss of electron energy, so the motion orbit of electron rotation around the nucleus can not be stable and continuous, and finally the electrons should fall into the nucleus due to the energy lose. However, this demonstration on the basis of classical electrodynamics theories is obviously not consistent with the fact; Secondly, the radiation generated by the accelerated electrons should be continuously distributed, which is inconsistent with the atomic spectrums that are discrete spectral lines; Thirdly, according to the classical theory, if the electromagnetic wave source emits a stream of wave with the specific frequency ν, it may also emit various harmonics with different frequencies concurrently, whose frequencies are the integer multiples of ν, but the experiment results of hydrogen atomic spectrum are inconsistent with this, because the frequency of spectral line results follows the principle of convergence (the spectral lines show a combination of different wave frequencies)[19].

Under this background, Bohr developed Planck's quantum hypothesis on the basis of the conclusions of hydrogen atomic spectrum experiment, leading to atomic quantum theory in 1913. There are two important hypotheses in Bohr quantum theory as following: Firstly, an atom has the attribute of discontinuous state when an electron rotates around the nucleus, so only when an electron orbit with angular momentum p equals to the integer multiples of h/2π, it is stable, which means that electrons rotate in the stable orbit. Under this state, electron possesses constant energy of $E_n$, and electron in the stable state does not absorb or emit radiation [19].

$$p = n \times \frac{h}{2\pi} \quad (n=1,2,3,..) \qquad \text{equation 31}$$

In this equation, n is the quantum number under the quantization condition. Secondly, electron switches to different orbits in the way of quantum transition: when an electron jumps from an orbit of stable state at energy $E_m$ to another orbit of stable state at energy $E_n$, the frequency ν of the absorbed or emitted photons is calculated as [19]:

$$\nu = \frac{E_n - E_m}{h} \text{ (frequency condition)} \qquad \text{equation 32}$$

According to Bohr's hypothesis, it is to calculate the electron orbital radius $a_n$ by applying classical mechanics, and then $a_n$ and the corresponding energy $E_n$ of the electrons in hydrogen-like atoms is expressed respectively as [19]:

$$a_n = \frac{n^2 a_0}{Z} \qquad \text{equation 33}$$

$$E_n = -\frac{\mu e_s^4 Z^2}{2n^2 h^2} \qquad \text{equation 34}$$

$$a_0 = \frac{h^2}{\mu e_s^2} \qquad \text{equation 35}$$

In this equation, $a_0$ is called the first Bohr orbital radius of the hydrogen atom; μ is the mass of electron; in the International System of Units (SI), $e_s = e\ (4\pi\varepsilon_0)$ -12, and e is the value of the electron charges (electron charge is -e); $\varepsilon_0 = 8.854\times10^{-12}\ C^2/N\cdot m^2$, in the Unit System of cm·gram·second (CGS), $e_s = e$; Z is the atomic number [19].

Consequently, the circular orbital radius of hydrogen atoms and the energy of hydrogen atoms can only be estimated as a series of discontinuous values, which are all quantized, and these discontinuous values of energy are usually called as energy levels of circular orbital. Experiments show that not only the energy of the hydrogen atoms, but also all other element atoms are quantized [19].

According to Bohr's frequency condition, the spectral frequency of hydrogen atom can be deduced into:

$$\nu = \frac{E_n - E_m}{h} = \frac{\mu e_s^2}{4\pi h^3}\left(\frac{1}{n'^2} - \frac{1}{n^2}\right) \qquad \text{equation 36}$$

Among which both n' and n are the energy levels of hydrogen atomic orbitals [19]. This equation quantifies the spectral frequency of electromagnetic waves absorbed or emitted by electron, when the electron switches from lower energy orbitals to higher energy orbitals or from higher energy orbitals to lower energy orbitals, respectively.

It is to input the Rydberg constant (ķ) into the above equation of Bohr's frequency condition, then it is completely consistent with Balmer formula that is used to represent the wavelengths of hydrogen atomic spectral line [19] [22]. By measuring the values of μ, e, $\varepsilon_0$, c and h in experiment, the calculated Bohr's frequency (ν) is well consistent with the experiment measurement results. After that, this Bohr's atomic

quantum model is further developed, suiting the elliptic shape orbitals of electron. By proposing the quantum model, the questions of microscopic particle motion can be quantitatively solved by adopting a combination of both classical mechanics and discontinuous quantized orbital equation [19].

### 4.6.Double-slit experiment between classical mechanics and electron

In the theory of classical mechanics, the state of a particle is described by the physical quantities of momentum and spatial position (vector), both of which can be measured independently. However, this calculation is not applicable on the microscopic particles due to the wave-particle duality of microscopic particles in quantum mechanics. As both the vector position and momentum of microscopic particles cannot be determined, how to quantify the wave-particle duality by using a physical quantity to describe the motion state of the microscopic particles? In 1926, Born attempted to explain the statistical nature of de Brogyi wave, who believed that de Brogyi wave did not represent the fluctuation of real physical quantity like classical waves, so it was a kind of probability wave that described the probability distribution of particles in space. To clarify this concept, the double-slit diffraction of electron experiment was conducted and the results was interpreted from the perspective of both ‘particles’ and ‘fluctuations’ to find out the connection between the two [19].

In order to better understand the the wave-particle duality of electrons in double-slit diffraction, it is first to compare the results of double-slit experiments between classical particles (e. g., sand) and classical waves (e. g., acoustic and water waves). For the classical particles passing through the double seams (S1 and S2): when only the seam S1 is opened, the spatial distribution of particle density is described by the wave figure of I1 after passing through the S1; when only the seam S2 is opened, the spatial distribution of particle density is described by the wave figure of I2 after passing through the S2; when the double seams of both S1 and S2 are opened concurrently, the spatial distribution of particle density through the S1 and S2 seams are completely added as: $I = I1 + I2$. However, for the classical waves passing through the double seams, the wave interaction between both is not simply added: when only S1 seam is opened, the spatial distribution of the wave intensity is described by the wave figure of I1 after the wave passes through the S1; when only S2 seam is opened, the spatial distribution of the wave intensity is described by the wave figure of I2 after the wave passes through the S2; when the double seams of both S1 and S2 are opened concurrently, the spatial distribution of wave intensity through both S1 and S2 seams are NOT completely added as $I = I1 + I2$, but are expressed as $I = I1+I2+2\times I1\times I2\times\cos\delta$, among which $\delta$ is the phase difference between the two waves independently passing through S1 and S2. Due to the existence of interference terms ($2\times I1\times I2\times\cos\delta$), the classical wave intensity distribution is different from the classical particle density distribution [19].

Next it is to analyze the electrons’ double-slit diffraction experiments on the basis of conclusions drawn from the classical particles and waves. When the electron beam

passes through the double slits, if the incoming flow of electron beam is weak, the electrons pass through the double slit almost one by one and subsequently hit the photosensitive screen. When the photosensitive time is short, it seems that the distribution pattern of the screen light dots is random and irregular. Nevertheless, when photosensitive time is prolonged enough, the screen light dots become more and more, and the distribution of screen light dots in some places become very dense, while in other places they are very thin and even in some places they are almost disappearing, so the final electronic screen distribution forms regular interference pattern. The distribution pattern of electron beam intensity is similar to the classic waves, but is different from the classical particle distribution pattern. In the above experiments, the pattern of diffraction is independent of the intensity of the incident electron flow. When the electron flow intensity is weaken to the state that almost the electrons are emitted one by one, the initial distribution pattern of screen light dots appears to show some irregular spots. However, as long as prolonged enough time, the same interference stripe as classical waves is still obtained on the photosensitive screen, showing the fluctuation of the electron. Therefore, it can be concluded that each particle diffracts independently of other particles, which means that diffraction is not the result of the interaction between these different particles and fluctuation is possessed by each microscopic particle, so each particle shows the nature of both particle and fluctuation. From the particle theory aspect, the peak intensity value in the interference pattern means that the electron projection probability is high, while there are few or no particles density at the minimum value; From the perspective of fluctuation theory, the intensity of the wave at the maximum in the interference pattern is great, and the intensity of the wave at the minimum is extremely small or even zero. Based on the theory of both particles and fluctuation, Born proposed statistical interpretation of the wave function, describing that the intensity of the wave function (the square of the absolute value of amplitude) at a point in space is proportional to the probability of particle occurrence at that point [19].

### 4.7.Wave-particle duality of de Broglie wave

Overall, the wave nature of microscopic particles is based on the statistics only, so it is to clarify the difference between classical waves and microscopic quantum waves: classical waves are usually defined as the transmission of substances in vibration forms. For this reason, there are two vectors of physical movements that need to be clarified in waves: the first movement vector is the vibration motion, and the second movement vector is the transmission motion, but what substance gets transmitted is the key to classify these waves. Based on the definition of two movement vectors in waves, it is easily to compare and contrast the classical wave nature with the microscopic quantum particles: for example, sound waves involve the up-and-down vibrations of air, but the air itself cannot move horizontally and only the ‘displacement’ from these up-and-down vibrations is transmitted horizontally. However, not all waves require the medium to transmit their ‘displacement’; for instance, electromagnetic waves would not need the medium and is capable of propagating directly through the vacuum. In comparison to the classical waves, the

waves of microscopic quantum particles also do not require the medium, but they transmit 'probability' by itself, which means that probability of particle occurrence is vibrating and this vibration is not identical to a kind of vertical displacement of particles in space, so it is just a type of mathematical 'vibration.' To put it further, probability waves can be understood as: the 'probability values' of microscopic particles are constantly vibrating in the spatial positions (or velocities), and what gets transmitted is the 'probability' itself, a mathematical value, other than the physical quantity [19].

In experiments, phenomena such as light and electrons sometimes behave like waves but in other times display like particles, so these phenomena exhibit wave-particle duality, but it is impossible to observe both wave and particle properties simultaneously. These phenomena are explained as: when an object's de Broglie wavelength is comparable to the particle size or exceeds its size, its wave nature can be detected, which thus cannot be ignored. However, if its de Broglie wavelength is much smaller compared to its particle size, then the particle object's wave nature cannot be detected at all. Consequently, it is proposed that the theories of both particles and waves nature can be applicable on the microscopic quantum particles as complementary explanations [19].

### 4.8.The mathematical expression of classical wave and quantum wave

The physical properties of the wave function are expressed mathematically below: it is described that the wave function of $\Phi(x, y, z, t)$ is defined as the state of a particle at a spatial point A with coordinate (x, y, z) and time t. The intensity of the wave is defined as the magnitude of complex number

$$\left|\Phi\right|^2 = \Phi^* \times \Phi \qquad \text{equation 37}$$

where $\Phi^*$ is the complex conjugate of $\Phi$[19].

According to the statistical interpretation of the wave function, the probability of the particle occurrence at the spatial point A is defined as dW(x, y, z, t), which is proportional to the magnitude of complex number representing the spatial point A as $\left|\Phi_A(x, y, z, t)\right|^2$, so at time t in the volume unit of dr (dr = dx×dy×dz) where the spatial point A (x, y, z) is located at the center of this volume unit, the coordinate of this volume unit is expressed as x~x+dx, y~y+dy and z~z+dz, and the probability dW (x, y, z, t) of the particle occurrence at spatial point A is proportional to $\left|\Phi_A(x, y, z, t)\right|^2$, which is expressed as [19]:

$$dW(x,y,z,t) = C \times \left|\Phi_A(x, y, z, t)\right|^2 \times d\tau \qquad \text{equation 38}$$

In the formula, C is the proportional constant, so the probability of a particle occurrence in a volume unit at the point A (x, y, z) at time t is defined as the density of probability, $\omega(x,y,z,t)$, which can be calculated as [19]:

$$\omega(x,y,z,t) = dW(x, y, z, t)/dr = C \times \left| \Phi_A(x, y, z, t) \right|^2 \quad \text{equation 39}$$

As particles must appear in somewhere over the whole coordinate (space point A can be any point in coordinate axes), the sum of the probabilities, representing that particles will appear at all the points in the whole spatial coordinate, is equal to 1, which can be consequently calculated as [19]:

$$C \times \int_{\infty} \left| \Phi A(x, y, z, t) \right|^2 \times dr = 1 \quad \text{equation 40}$$

The infinity symbol of $\infty$ under the integral signs means to integrate the probability over all spatial points, so the proportional constant C is deduced by above equation as [19]:

$$C = 1/\left(\int_{\infty} \left| \Phi A(x, y, z, t) \right|^2 \times dr\right) \quad \text{equation 41}$$

Next it is to define the normalization of wave function as $\Psi(x,y,z,t)$, and then this wave function is derived from the magnitude of complex number and the proportional constant [19]:

$$\Psi(x,y,z,t) = C \times \Phi(x,y,z,t) = \Phi(x,y,z,t) /\left(\int_{\infty} \left| \Phi A(x, y, z, t) \right|^2 \times dr\right) \quad \text{equation 42}$$

The wave functions of both $\Psi$ and $\Phi$ describe the same state, and thus the probability of a particle occurrence in the volume unit of dr near the point (x, y, z) at time t is further expressed by the normalization of wave function [19]:

$$dW(x,y,z,t) = \left| \Psi(x, y, z, t) \right|^2 \times dr \quad \text{equation 43}$$

Then the density of probability in particle occurrence, $\omega(x,y,z,t)$, is further calculated by using normalization of wave function [19]:

$$\omega(x,y,z,t) = \left| \Psi(x, y, z, t) \right|^2 \quad \text{equation 44}$$

The sum of the probabilities, representing that particles will appear at all the points in the whole spatial coordinate, is also expressed by inputting normalization of wave function [19]:

$$\int_{\infty} \left| \Psi(x, y, z, t) \right|^2 \times dr = 1 \quad \text{equation 45}$$

The procedure of turning the wave function of $\Phi(x,y,z,t)$ into $\Psi(x, y, z, t)$ is called as the normalized process of quantum wave, and the proportional constant C is correspondingly defined as the normalization constant [19]. With regards to the above normalization procedure of wave functions, there are additional methods in adopting this normalized wave function under different scenarios:

Firstly, it is worthwhile noting that the above normalization of wave functions is not unique. For example, if Ψ is a normalized wave function, then the transformed wave function of $e^{i\delta}$ Ψ (where δ is any real constant) is also normalized. Consequently, the equation of $|\Psi|^2=|e^{i\delta}\times\Psi|^2$ means that $e^{i\delta}\Psi$ describes the same probability wave with the phase factor of constant $e^{i\delta}$, and a normalized wave function can contain any phase factor, so it is feasible to use this property of wave functions to simplify the complex wave functions via multiplying or dividing by a phase factor in the next [19].

Secondly, if the magnitude of complex number, $\int_\infty |\Phi|^2 \times dr$, diverges, meaning that the wave function is not square-integrable over all space, then this wave function cannot be normalized according to the above steps, as this wave function would result in a normalization factor C = 0, which is clearly meaningless. For example, if the wave function of a free particle is defined as Ψp (r,t) = A× Exp[$\frac{i}{h}$ × (p×r-E×t)] that has a modulus squared of $\Psi_p^2=\Psi_p^*\times\Psi_p=A^2$, then this constant C is independent of time and coordinates. This independent constant means that the probability of a particle occurrence in a unit volume near any spatial point is the same, which is expressed as equation: $\int_\infty |\Phi|^2 \times dr = A^2\int_\infty dr = \infty$. Consequently, such wave functions are not square-integrable over all space points and cannot be normalized according to the above steps [19].

Thirdly, if the state of a particle is described by the normalized wave function ψ(r, t), then the probability distribution function at spatial unit volume of r at time t is defined as ω(r, t) [19]:

$$\omega(r,t)\times dr = |\Psi(r,t)|^2 \times dr \qquad \text{equation 46}$$

Using the above formula, it is to calculate the average value of particle coordinates ($\bar{x}$) at x axis according to the common averaging equation by probability [19]:

$$\bar{x} = \int x\,|\Psi(r,t)|^2\,dr \qquad \text{equation 47}$$

Fourthly, if there is any mechanical quantity f(r) of a particle that is known, its average can be expressed as [19]:

$$\overline{f(r)} = \int \psi^* f(r)\,\psi\,dr \qquad \text{equation 48}$$

Finally, the complex number form of wave function cannot be directly measured experimentally in quantum mechanics, so its mathematical equations only refer to the probability of particle occurrence in space, which is discussed above. Then the philosophy of quantum mechanics maths is that the variable of any real mechanical

quantity of f(r) can be incorporated into this mathematical equation of occurrence probability.

### 4.9.The superposition of wave functions

In the linear system of classical physics, the linear differential equations (groups) are usually applicable on the physical quantities (including functions, vectors or vector fields) that meets the requirements of the linear equations (groups) describing their physical processes. For all the classical fluctuation processes, in which the principle of superposition is applicable, any fluctuation process φ is the result of the linear superposition of two possible fluctuation processes, φ1 and φ2, expressed as [19]:

$$\varphi = a\times\varphi 1 + b\times\varphi 2 \text{ (a, b are both constant)} \qquad \text{equation 49}$$

For classical waves that are driven by the superposition principle, such as water waves, acoustic waves, the synthetic amplitude of two or more waves propagating in the same space is the sum of the amplitudes generated separately by each wave. When the physical quantities are measured, only the amplitude of the synthetic variable is measurable, rather than the physical quantities generated separately by each wave, which means that its individual states participating in the superposition do not have their independent characteristics [19].

One of the main ways to calculate the physical quantities of a wave function is to sum the wave function as a superposition of some independent wave functions that are derived under particularly simple state, which is also called quantum superposition. For instance, because the Schrodinger wave equation is linear, the overall physical quantities of the wave function can be calculated on the basis of the superposition principle. In optics, the light interference and diffraction phenomenon can be explained by using the superposition principle: one beam of the incident electrons passes through slit S1 and the other beam passes through slit S2, represented by wave functions of ψ1 and ψ2 respectively [19].

The experimental results show that: the state of the particle after passing through the double slit is represented by the wave function of ψ, which is the result of the linear superposition of ψ1 and ψ2, calculated as [19]:

$$\psi = C_1\times\psi_1 + C_2\times\psi_2 \text{ ($C_1$ and $C_2$ can be any complex constants)} \qquad \text{equation 50}$$

Only in this superposition way, the interference phenomenon can be explained, because the superposition of the interference pattern on the screen is measured by the interference intensity as below [19]:

$$\left|C_1\times\psi_1 + C_2\times\psi_2\right|^2 = \left|C_1\times\psi_1\right|^2 + \left|C_2\times\psi_2\right|^2 + C_1C_2\times\psi_1^*\times\psi_2 + C_1C_2^*\times\psi_1\times\psi_2^*$$

equation 51

Among which $C_1C_2\times\psi_1^*\times\psi_2 + C_1C_2^*\times\psi_1\times\psi_2^*$ is the interference item, explaining the interference intensity variation of the superposition waves [19].

It is further to deduce the principle of state superposition in quantum mechanics from the equations of classical substance wave: If ψ1 and ψ2 are two possible states of the system, then their linear superposition of $\psi = C_1\times\psi_1 + C_2\times\psi_2$ ($C_1$ and $C_2$ can be any complex constants) is also a possible state of the system [19]. Consequently, the key difference in linear state superposition between quantum mechanics and classical substance wave is that the linear state superposition of quantum mechanics only refers to the superposition of probability under the same state, but the classical substance wave superposition is the superposition of physical quantities.

## 5.Schrodinger wave equation

### 5.1.The transformation of free particle plane wave function

As the equation to be established describes how the wave function of Ψ(r,t) changes over time variable of t at space unit volume of r, there are the following conditions to be met: Firstly, the equation is a differential equation of the first derivative to the wave function Ψ(r,t), with respect to the time variable of t, as it allows to determine the state at any given moment from the initial state of the microscopic system; Secondly, the equation is linear, meaning that if Ψ1 and Ψ2 are both solutions to this equation, and then their linear combination of aΨ1 + bΨ2 is also a solution, so the linearity of the equation ensures that its solutions are applicable on the principle of superposition; Thirdly, the coefficients in the equation (such as constant a and b) should not contain any parameters describing physical state quantities such as energy or momentum [19].

By clarifying the above pre-conditions, it is to convert the free particle plane wave function of Ψ(r,t) into Schrodinger wave equation and the conversion steps are deduced below [19]:

The free particle plane wave function of ψ(r,t) is expressed as:

$$\psi(r,t) = A\times\exp[\frac{i}{\hbar}\times(p\times r - E\times t)] \qquad \text{equation 52}$$

Where the space unit volume of r is near the spatial point with coordinates (x,y,z), so it can be re-expressed as:

$$\psi(x,y,z,t) = A\times\exp[\frac{i}{\hbar}\times(p_x\cdot x + p_y\cdot y + p_z\cdot z - E\cdot t)] \qquad \text{equation 53}$$

Where $p_x$ ,$p_y$ , $p_z$ is the momentum vector at x, y, z axis, respectively [19].

It is first to take the partial derivative of time variable t on the basis of ψ(x,y,z,t):

$$\frac{\partial \psi}{\partial t} = - \frac{i}{\hbar} \times E \times \psi \qquad \text{equation 54}$$

Then it is to calculate the second partial derivatives at coordinates x, y, z respectively:

$$\partial^2\psi/\partial x^2 = - (p_x^2/\hbar^2) \times \psi$$

$$\partial^2\psi/\partial y^2 = - (p_y^2/\hbar^2) \times \psi \qquad \text{equation 55}$$

$$\partial^2\psi/\partial z^2 = - (p_z^2/\hbar^2) \times \psi$$

It is to further integrate three equations of second partial derivatives into a whole:

$$(\partial^2/\partial x^2 + \partial^2/\partial y^2 + \partial^2/\partial z^2)\times\psi = - (p^2/\hbar^2) \times \psi \qquad \text{equation 56}$$

Where the parameter of $(\partial^2/\partial x^2 + \partial^2/\partial y^2 + \partial^2/\partial z^2)$ is replaced by the symbol of $\nabla^2$, which is re-named as Laplacian operator in Euler's method [19].

**5.2.The operator and Schrodinger equation**

To integrate the relationship of a free particle between the energy E (kinetic energy) and momentum p, $E=p^2/2\mu$, where μ is the mass of the particle, the equation is derived into [19]:

$$E\times\psi = i\hbar\times\frac{\partial \psi}{\partial t} \qquad \text{equation 57}$$

$$(p\cdot p)\times\Psi = (-i\hbar\nabla\,)(-i\hbar\nabla)\times\Psi \qquad \text{equation 58}$$

In this formula, the symbol of ∇ is called as Nabla operator in Euler's method (Please note: as the imaginary unit, $i^2 = -1$; $1/i = 1$ in this deducing process) [19].

$$\nabla = i\times\frac{\partial}{\partial x} + j\times\frac{\partial}{\partial y} + k\times\frac{\partial}{\partial z} \qquad \text{equation 59}$$

Where i, j, k is the imaginary unit at x, y, z axis respectively [19].

By introducing the Nabla operator, both energy E and momentum p of a particle are expressed as the following operators acting on the wave function [19]:

$$E \rightarrow i\hbar\frac{\partial}{\partial t} \qquad p \rightarrow -i\hbar\nabla \qquad \text{equation 60}$$

From this formula, it is to replace the energy and momentum variables by the Nabla operators of Euler' method in the classic energy-momentum relationship, and then to apply them on the wave function Ψ, so the wave equation for a free particle can be obtained. For a particle in the given potential field of U, it is to define the potential

energy of the particle under the force field to be U(r), and the total energy of the particle becomes the sum of both kinetic and potential energy [19]:

$$E = \frac{p2}{2\mu} + U(r) \qquad \text{equation 61}$$

Replacing the physical properties of both E and p in the above formula by Nabla operators, then the wave function is re-expressed as [19]:

$$i\hbar \times \frac{\partial \psi}{\partial t} = [- \frac{\hbar 2}{2\mu} \times \nabla^2 + U(r)] \times \Psi \qquad \text{equation 62}$$

This equation is called the Schrodinger wave equation, which usually refers to the time-dependent Schrodinger equation, and it describes the variation of particle state with the time change under the potential field of U(r). If the force field acting on the particle wave varies with time variable of t, the general form of the above equation is calculated as [19]:

$$i\hbar \times \frac{\partial \psi}{\partial t} = [- \frac{\hbar 2}{2\mu} \times \nabla^2 + U(r,t)] \times \Psi \qquad \text{equation 63}$$

It is hypothesized that the force field acting on the particle does not change over time, and then the potential energy formula of U(r) does not include the time variable of t. Under this situation the wave function is called stationary state. It is to re-define the wave function of Ψ(r,t) by dividing it into the sub-function (ψ(r)) of variable r and the sub-function (f(t)) of variable t separately [19]:

$$\Psi(r,t) = \psi(r) \times f(t) \qquad \text{equation 64}$$

Then it is to derive the particular integral of the Schrodinger equation [19]:

$$\Psi(r,t) = \psi(r) \times \text{Exp}(- \frac{i}{\hbar} Et) \qquad \text{equation 65}$$

The relationship between this wave function and time t is sinusoidal, with its angular frequency of ω = E/ħ. It can be seen from De Broglie's equation that the constant E is the energy of the system under the stationary state, so its corresponding micro-particles' state is also stationary described by this wave function, including:

The potential energy U(r) of the particle is independent of time variable t, and the energy E is given a constant value [19].

The probability density of a particle occurrence ($|\Psi(r,t)|^2$) is independent of time, indicating that the probability distribution of a particle does not change over time. The equation is expressed as [19]:

$$|\Psi(r,t)|^2 = \left|\psi(r) \times \mathrm{Exp}\left(-\frac{i}{\hbar}Et\right)\right|^2 = |\psi(r)|^2 \qquad \text{equation 66}$$

The average of any mechanical quantity does not change over time, which means that the time variable is not included in the functions of any mechanical quantity mean value [19].

To fully describe the motion state of an electron, there are four quantum variables that must be required, including the principal quantum number, angular quantum number, magnetic quantum number and spin magnetic quantum number, among which the first three variables are all the solutions of Schrodinger equation, except that spin magnetic quantum number is not a solution of Schrodinger equation. Both principal quantum number and angular quantum number are related with electron energy, while magnetic quantum number characterizes the electron angular momentum [23].

## 6.Further development of mechanics models in this article

**6.1.**Mechanical movement refers to the vector variation in the displacement of the mass point in matter both temporally and spatially, which is different from the movement of matter existing as energy only. According to the new definition of photon in my another quantum physics article [13], this article proposes that photons are the most elementary research object for mechanical motion, which are also the smallest partitioning mass unit of mass matter, so the natural Law of electromagnetic wave particle duality is a basic attribute of mass matter, not limited to the basic properties of energy matter.

**6.2.**According to the Figure 1 of my article [11], it is to further discuss the argument of the shielding effect of the electric field inside an atom and its effects on the electron orbitals:

**6.2.1.**For the adjacent atoms of the same element, the frequency of the electromagnetic waves generated by adjacent atoms is the same, so interference waves of electromagnetic waves are easily formed between adjacent atoms;

**6.2.2.**Multiple equipotential lines are formed between the zones of constructive interference and the zones of destructive interference. The destructive interference zone is relatively neutral due to the offsetting between wave peaks and bottoms, and electrons tend to undergo rotation motion in the destructive interference zones, thus becoming an important factor affecting the electron rotation orbit. In the motion model shown in Figure 1, the shielding effect of the electric field inside the atom causes the electron orbitals to be relatively fixed rather than the randomly disordered orbitals;

**6.2.3.**Electrons tend to rotate in the outer space of a closed circular equipotential line, which meets the pre-conditions for the formation of electric field shielding.

**6.3.**To compare and contrast with the shielding effect of electric field inside an atom, macroscopic celestial bodies (such as stars and planets) also have field shielding effects inside them. However, unlike the shielding effect inside microscopic atoms, macroscopic celestial bodies mainly rely on the substance boundary layers to form field shielding effects. The rupture of the boundary layer leads to the destruction of the shielding effect, which is the main factor causing various natural disasters such as tornadoes, earthquakes, solar flares, etc [6][7][8]. Therefore, the stable boundary layer and the generated field shielding effect is the important influencing factor in the development motion of celestial bodies. Similar to the internal equipotential lines of microscopic atoms, the overall equipotential lines inside celestial bodies tend to form closed loops. Due to the shielding effect generated by equipotential lines, substances move parallelly to the equipotential lines in both sides [12]. This motion model is the main factor that enables celestial bodies in our three-dimensional space to evolve into regular spherical shapes.

**6.4.**It is to re-analyze the wave-particle duality of de Broglie wave below:

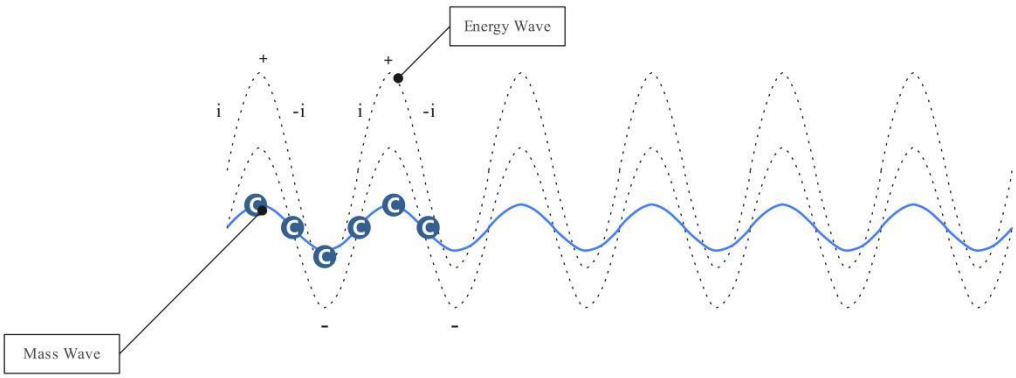



**Figure 6. De Broglie wave: The quantum wave of elementary particles.**

My article re-defines the classical material wave as mass wave, and it is to divide the De Broglie wave generated by elementary particles into two components, including mass wave and energy wave (both electric and magnetic field energy) shown in Figure 6. Then the difference in physical quantities is critically compared between classical material wave and quantum wave in the Table 1.

**Table 1. Comparison between classical material wave and quantum wave.**

| | Classical material wave | Quantum wave |
|---|---|---|
| Wave type | Mass wave | Mass wave and energy wave (both electric and magnetic field energy) |
| Energy form transmitted by wave | Kinetic energy | Kinetic energy and electromagnetic energy |
| Interaction form between two waves | Collisions among particles of two mass waves | Through wave nature of dark matter driven by two waves |
| The product of two waves' interaction | Interference wave by two mass waves | Interference wave by two mass waves; Interaction between positive and negative poles of two energy waves |

Under the hypothesis that De Broglie wave is divided into mass wave and electromagnetic energy wave, the wave-particle duality of de Broglie wave can be easily understood: de Broglie wave does not only possess the same attributes of mass particles as the classical material wave, but also shows the physical quantities of electromagnetic energy wave that is generated and carried by the beam of elementary particles (photons, electrons, proton...) at quantum level. Consequently, the wave functions of mass wave and electromagnetic energy wave need to be calculated separately for de Broglie wave next.

It is to give the imaginary unit of 'i' the realistic attribute: the imaginary unit of 'i' represents the phase of De Broglie wave (shown in Figure 6), and when two micro-particles undergo wave motion in the same phase, the poles of electromagnetic wave show the same nature, so the interaction product of two micro-particles is to generate the repelling force, expressed as the mathematical equation, $i^2 = -1$. Under this hypothesis, the imaginary unit of 'i' is given the realistic nature, rather than just facilitating the mathematics calculation.

**6.5.** In summary, this paper firstly reviews the classical principles of mechanics, and classical mechanics can effectively solve physics cases under the common limitation conditions, that include macroscopic physical conditions and low-speed motion model. However, under the situations of quantum micro-scale, cross-galaxy motion models and material aging process, new physical models need to be established to solve physical problems. My previous papers have fully discussed the particle collision motion model at microscopic quantum field [1], the microscopic quantum mechanics model under the electric field shielding effects of the overall atomic structure [10], the force balance analysis at each mass point inside an atom[2][3], inter-molecule force generating sources [4], thermal motion model of micro particles in the process of materials aging [5][9], friction resistance model at quantum scale [4], charged

particles motion model under free state at the substance boundary layers in nature [6][7], dark matter principle and its application on inter-galactic motion model [8], etc. Therefore, Table 2 fully summarizes the original mechanics models proposed by my previous articles as well as by this current article.

**Table 2. Summary of mechanics models originally proposed in our sponsored journals.**

| Scope level | Mechanics model | References |
|---|---|---|
| Elemental particle level | The particle collision motion model | [1]; Figure 4 of this article. |
| Elemental particle level | Mechanics model under the electric field shielding effects of the overall atomic structure | [10]; Section 6.2 of this article. |
| Elemental particle level | The force balance analysis at each mass point inside an atom | [2];[3]. |
| Elemental particle level | The conduction of thermal motions among elementary particles (both electrons and protons) | [32]. |
| Elemental particle level | The resonant state of metastable composite nucleus and gravitational wave generation | [8]. |
| Atomic or molecular level | Inter-molecule force generating sources | [4]. |
| Atomic or molecular level | Thermal motion model of micro particles in the process of materials aging | [5];[9]. |
| Atomic or molecular level | Friction resistance model at quantum scale | [4]. |
| Atomic or molecular level; Macro materials level | Charged particles motion model under free state at the substance boundary layers in nature | [6];[7]. |
| Macro planet or star level | Both parallel and vertical convection motions along the substance boundary layers forming field shielding effects of a planet or star. | [6];[7];[8];[12];[30]. |
| Astronomic level | Dark matter principle and its application on | [8]. |

| | | |
|---|---|---|
| | inter-galactic motion model | |
| Astronomic level | The magnetism along the fourth dimensional space and the driving force of celestial rotation | [18]. |

## 7.Experiment methods

### 7.1.Particle collider data

The basic structure and operation mechanism of particle collider instrument have been introduced in my another article [13]. This article systematically collects the particle collision data from several research projects that are produced by Beijing Electron Positron Collider (BEPC), which have been published in China. Consequently, these particle collision data are comparable due to the generation by the same instrument, although these data are analyzed by different research teams. The Beijing Electron Positron Collider (BEPC) is a high-luminance collider of $e^-e^+$ with multiple beam bunches, designed to specifically study the physical processes in the r-charm energy region. Its main parts consist of an injector, a beam transport system, and a storage ring. To achieve its scientific goals and meet the technical requirements of the BEPC, the Beijing Spectrometer must satisfy specific conditions below: high-precision recording of the position, velocity and energy of both charged and neutral particles; high-resolution for the measurement of energy and angular velocity, especially for electrons and photons; high-resolution for measuring momentum and time to improve the analysis of charged particles; a front-end electronics system and data acquisition system that can be adapted to multi-beam bunch modes; excellent particle recognition capabilities, particularly for T, K, and P particles; and high-precision software for offline simulation, reconstruction, and calibration. The specific parts are mainly composed of main drift chamber (MDC), time of flight counter (TOF), electromagnetic calorimeter (EMC), muon discriminator (MUC) and other sub-detectors, hardware (such as the superconducting magnet) and software systems used for particle and event identification [36].

The main function of the MDC is to use gas amplifiers and wire detectors to measure the trajectories and electric charges of particles, which are essential in particle identification, including the measurement of both trajectory and momentum of final-state charged particles. According to its function, this instrument can be categorized into time measurement and charge measurement; The TOF method measures the duration of $\Delta t$ from the particle's generation source to the detector, in combination with the measured flight path length (L) and momentum (P), to determine the intrinsic mass ($M_0$) of the particle; The EMC part primarily measures the energy of both charged particles such as electrons and neutral particles such as photons, consisting of a barrel calorimeter and an end calorimeter; The Muon discriminator (MUC) is designed to identify Muons and distinguish Muons from $\pi$ mesons; The superconducting magnet provides the uniform magnetic field with

high-intensity, enabling precise measurement of the momentum information for high-momentum particles [36].

Finally, the collected particle collision data are adapted by the estimation of observation on the basis of published Figures, summarized in Table 3, Table 4 and Table 5.

### 7.2. Quantum wave experiment and simulation

The electron wave diffraction experiment and double-slit experiment are introduced in above review content to analyze the quantum wave theories. Correspondingly, to further explore the relevant scientific findings, this article selects the interferometer experiment and empirical modeling of electron diffraction in transmission electron microscopy (TEM) to conduct the observation study project.

Zeng Zi-Qi conducted spectral studies by using three types of interferometers, including the HOM interferometer, N00N interferometer and Franson interferometer. In addition to fundamental research, these three types of interferometers also play a crucial role in various industrial applications, which are capable of precisely measuring optical properties such as wavelength, phase, amplitude, coherence and polarization. An improved interferometer of HOM, which are consisted of two polarization beam splitters (PBS), two reflectors and two halfwave plates (HWP), has been designed in this research. To gain the deeper understanding of the relationship between HOM interference and N00N interference, controllable transformations were demonstrated between HOM interference and N00N interference under the same experimental setup. In order to study the spectral-time characteristics and resolve Franson interference both theoretically and experimentally, it is to compare the interference patterns of frequency-positive correlated, frequency-negative correlated, and uncorrelated two-photon states, which offers a new perspective on understanding the spectral-time characteristics of the Franson interferometer [39].

Electron diffraction is the crucial technique part in transmission electron microscopy (TEM). As the incident wavelength of electrons' beam wave in TEM is typically much shorter than that of X-rays used for diffraction experiments, the Ewald sphere radius of electron diffraction becomes significantly larger, which allows more reciprocal lattice points to interact, generating additional diffraction beams, so it reveals more crystalline information. The most representative technique in TEM is named as selective area electron diffraction (SAED), which produces diffraction patterns through parallel illumination of electron beams. There are both relativity dynamics model and relativity motion model compared in this research. It is worthwhile mentioning that the parameters used in dynamics model are based on the empirical measuring data and is widely applied in practice, while the motion model is the theoretical model only [40].

The spectral characteristics results are summarized in Table 6 by observation

estimation on the experimental figure results; the diffraction pattern data are drawn in Figure 7 ~ Figure 12 on the basis of observational estimation on the modeling graph.

## 8. Particle mass, momentum and energy in the particle collision process

In this section, my article characterizes the physical quantities of particle mass, momentum and energy in the decaying chain of particle collision experiment, with emphasis of these parameters: mass/energy/momentum range along which the events distribute, mass/energy/momentum level at which the peak events occur, amount of peak events.

### 8.1. Case studies

BABAR collaboration team measured the produced cross section of $e^+e^- \rightarrow Ø\eta$ decaying process by using the initial state radiation method, and observed the decay process of $e^+e^- \rightarrow \eta'Ø$ during the study of particle decaying process: $e^+e^- \rightarrow K^+K^-\pi^+\pi^-\pi^0$, but due to the small amount of events in the $e^+e^- \rightarrow \eta'Ø$ decaying process, further research could not be carried out. Subsequently, the BEIII collaboration team studied the invariant mass spectrum of $Ø\eta'$ through the process of $J/\Psi \rightarrow \eta Ø\eta'$, observing the existence of resonant states with statistic significance of $5\sigma$, as the complement to the BABAR team's findings [32].

Indicated by both BABAR and BEIII research team, Sun Yan-kun (2019) subsequently conducted the experiment analysis to study the decaying process of both $K^+K^-$ and $\pi^+\pi^-\gamma$ at energy level of 2125 MeV, which was able to clearly observe the signals of decaying process: $e^+e^- \rightarrow Ø\eta'$, although there were massive background events appearing in the collision experiment [32]. However, Sun Yan-kun's study has only outlined the results by figures, without describing the data in more detail, so my article tries to further analyze the experiment data that are estimated according to this study's figures and are summarized for comparison in Table 3.

Ban Zhenglin (2020) studied the recoil invariant mass spectrum of particle state of both $\pi^+\pi^-$ and $\pi^+\pi^-\pi^0$ in the decaying chain of $\Psi(2S) \rightarrow \pi^0 h_c$ ($h_c \rightarrow 3(\pi^+\pi^-)$), and the Gaussian fitting optimization results were further analyzed according to the background data. Additionally, the invariant mass spectrum of double photons was recorded as the background data for analysis in this research. Another decaying chain studied by this research was $J/\Psi \rightarrow \gamma 3(\pi^+\pi^-)$, in which particle states of both $\gamma\gamma$ and $3(\pi^+\pi^-)$ were recorded for the invariant mass spectrum by screening the 'noise' of event samples [33].

Pan Xiang (2019) studied in total 9 decaying pathways, aiming to systematically analyze the hadronic decaying characteristics of D meson, whose data were provided by BESIII collaboration team under the particle collision conditions of $\Psi(3770)$. These nine decaying pathways include $\overline{D} \rightarrow K^+\pi^-$, $\overline{D} \rightarrow K^+\pi^-\pi^0$, $\overline{D} \rightarrow K^+\pi^-\pi^-\pi^+$, $D^- \rightarrow K^+\pi^-\pi^-$, $D^- \rightarrow K_S^0\pi^-$, $D^- \rightarrow K^+\pi^-\pi^-\pi^0$, $D^- \rightarrow K_S^0\pi^-\pi^0$, $D^- \rightarrow K_S^0\pi^-\pi^-\pi^+$, $D^- \rightarrow K^+K^-\pi^-$[34].

Zhang HongHong (2019) studied the decaying pathway of $\Psi(3686)\rightarrow\Lambda\bar{\Lambda}\omega$, and $\Lambda$ baryon was electrically neutral and composed of quark 'uds'. However, $\Lambda$ baryon was further decayed into the final particle states through four kinds of pathways: $\Lambda\rightarrow p\pi^-$, $\bar{\Lambda}\rightarrow\bar{p}\pi^+$, $\omega\rightarrow\pi^+\pi^-\pi^0$, $\pi^0\rightarrow\gamma\gamma$, which included 6 charged particles ($\pi^+\pi^+\pi^-\pi^-p\bar{p}$) and two photons ($\gamma\gamma$). Another decaying pathway of $J/\Psi\rightarrow\Lambda\bar{\Lambda}\eta$ was also studied, whose final particle states included four charged particles ($p\bar{p}\pi^+\pi^-$) and two photons ($\gamma\gamma$) via three decaying sub-pathways: $\Lambda\rightarrow p\pi^-$, $\bar{\Lambda}\rightarrow\bar{p}\pi^+$, $\eta\rightarrow\gamma\gamma$[35]. The mass range, mass level at peak events and peak events amount of these final state particles were selected by my article and summarized in Table 3 (24)~(30).

Subsequently, Zhang HongHong (2024) further collected the particle collision data produced in 2021, aiming to analyze the excited state of $\Lambda$ baryon in the decaying pathway of $\Psi(3686)\rightarrow\Lambda\bar{\Lambda}\omega$. The invariant mass spectrum of final particle states, including $p\pi^-$, $\bar{p}\pi^+$, Recoil $\pi^+\pi^-$, $\pi^+\pi^-\pi^0$, was selected and fitted in this study. In addition to the data of decaying pathway $J/\Psi\rightarrow\Lambda\bar{\Lambda}\eta$ produced in 2009 and 2012, his study also collected the data of the same decaying pathway generated from 2017 to 2019 with approximately $8774\times10^6$ events detected in total. Four charged particles in forms of both $p\pi^-$ and $\bar{p}\pi^+$, as well as two photons, were analyzed in this decaying pathway [36].

Wu XiongHao (2024) studied the decaying chain of $\tau^+\tau^-\rightarrow K^+K^-K^\pm\mu^\pm\mu_\mu(\bar{\mu}_\mu)\bar{\mu}_T\mu_T$ at energy level of 3686 MeV. In total four types of final particle states were found in this particle collision research, including $\mu$, $K^+K^-K^\pm$, all of which were electrically charged particles. Particle's momentum during each particle decaying chain and total particle energy were analyzed under different assumed limitations for calculation, according to the collision data collected from BEIII research team in 2009, 2012 and 2021. The criteria of $\chi_\mu$ was introduced to screen the raw data, and $\chi_\mu$ referred to the application of $\mu$ particles on theoretical calculations, expressed as [37]:

$$\chi_\mu = [dE/dx\ (\text{theoretical expectation}) - dE/dx\ (\text{actual measurement})]/(\text{detector resolution})$$

equation 67

Where variables of E and x represented the energy and position along the decaying chain, respectively [37].

### 8.2. Results and description

**Table 3. Summary of particle's mass during particle decaying process.**

| Decaying process | Mass range | Mass at peak events | Peak Events |
|---|---|---|---|
| (1) $J/\Psi\rightarrow\gamma\emptyset\eta'$ | 1.96 ~ 2.56 ($GeV/C^2$) | 2.11 ($GeV/C^2$) | 90 (20 $MeV/C^2$) |
| (2) $J/\Psi\rightarrow\eta\emptyset\eta'$ | 1.96 ~ 2.56 ($GeV/C^2$) | 2.38 ($GeV/C^2$) | 35 (20 $MeV/C^2$) |

| | | | |
|---|---|---|---|
| (3) $K^+K^-$ | 1.0 ~ 1.8<br>(2125 MeV) | 1.02<br>(2125 MeV) | 710<br>(0.004 GeV/$C^2$) |
| (4) $\pi^+\pi^-\gamma$ | 0.3 ~ 1.1<br>(2125 MeV) | 0.77<br>(2125 MeV) | 540<br>(0.004 GeV/$C^2$) |
| (5) $K^-\pi^+$ | 0.62~1.20<br>(2125 MeV) | 0.90<br>(2125 MeV) | 580<br>(0.003 GeV/$C^2$) |
| (6) $K^+\pi^-$ | 0.62~1.20<br>(2125 MeV) | 0.90<br>(2125 MeV) | 590<br>(0.003 GeV/$C^2$) |
| (7) $\pi^+\pi^-$ | 0.28~1.05<br>(2125 MeV) | 0.50<br>(2125 MeV) | 820<br>(0.004 GeV/$C^2$) |
| (8) Ø | 0.985~1.17<br>(3097 MeV) | 1.02<br>(3097 MeV) | 6400<br>(0.001 GeV/$C^2$) |
| (9) $\pi^+\pi^-\gamma$ | 0.9~1.1<br>(3097 MeV) | 0.955<br>(3097 MeV) | 2300<br>(0.001 GeV/$C^2$) |
| (10) $\pi^+\pi^-$ | 1.0~3.5<br>(3686 MeV) | 3.10<br>(3686 MeV) | 3000<br>(0.0125 GeV/$C^2$) |
| (11) Double Photons | 0~0.16<br>(3686 MeV) | 0.13<br>(3686 MeV) | 8900<br>(0.003 GeV/$C^2$) |
| (12) $\pi^+\pi^-\pi^0$ | 0.4~2.8<br>(3686 MeV) | 0.8<br>(3686 MeV) | 4200<br>(0.013 GeV/$C^2$) |
| (13) $\gamma\gamma(J/\Psi\rightarrow\pi^0 3(\pi^+\pi^-))$ | 0.02~0.20<br>(GeV/$C^2$) | 0.135<br>(GeV/$C^2$) | 1900<br>(0.004 GeV/$C^2$) |
| (14) $\gamma\gamma(J/\Psi\rightarrow\gamma 3(\pi^+\pi^-))$ | 0.02~0.20<br>(GeV/$C^2$) | 0.18<br>(GeV/$C^2$) | 1100<br>(0.004 GeV/$C^2$) |
| (15) $\overline{D}\rightarrow K^+\pi^-$ | 1.862~1.872<br>(GeV/$C^2$) | 1.866<br>(GeV/$C^2$) | 45000<br>(0.00025GeV/$C^2$) |
| (16) $\overline{D}\rightarrow K^+\pi^-\pi^0$ | 1.84~1.88<br>(GeV/$C^2$) | 1.865<br>(GeV/$C^2$) | 66000<br>(0.00025GeV/$C^2$) |
| (17) $\overline{D}\rightarrow K^+\pi^-\pi^-\pi^+$ | 1.84~1.875<br>(GeV/$C^2$) | 1.865<br>(GeV/$C^2$) | 58000<br>(0.00025GeV/$C^2$) |
| (18)$D^-\rightarrow K^+\pi^-\pi^-$ | 1.865~1.875<br>(GeV/$C^2$) | 1.87<br>(GeV/$C^2$) | 70000<br>(0.00025GeV/$C^2$) |
| (19)$D^-\rightarrow K_s^0\pi^-$ | 1.865~1.875<br>(GeV/$C^2$) | 1.87<br>(GeV/$C^2$) | 8000<br>(0.00025GeV/$C^2$) |
| (20) $D^-\rightarrow K^+\pi^-\pi^-\pi^0$ | 1.835~1.885<br>(GeV/$C^2$) | 1.87<br>(GeV/$C^2$) | 20000<br>(0.00025GeV/$C^2$) |
| (21)$D^-\rightarrow K_s^0\pi^-\pi^0$ | 1.835~1.885<br>(GeV/$C^2$) | 1.87<br>(GeV/$C^2$) | 14000<br>(0.00025GeV/$C^2$) |
| (22)$D^-\rightarrow K_s^0\pi^-\pi^-\pi^+$ | 1.835~1.885<br>(GeV/$C^2$) | 1.87<br>(GeV/$C^2$) | 11000<br>(0.00025GeV/$C^2$) |
| (23)$D^-\rightarrow K^+K^-\pi^-$ | 1.835~1.885<br>(GeV/$C^2$) | 1.87<br>(GeV/$C^2$) | 6500<br>(0.00025GeV/$C^2$) |
| (24)$p\pi^-$ | 1.100~1.130<br>(GeV/$C^2$) | 1.116<br>(GeV/$C^2$) | 45<br>(0.0002GeV/$C^2$) |

| | | | |
|---|---|---|---|
| (25)$\bar{p}\pi^+$ | 1.100~1.130 (GeV/$C^2$) | 1.116 (GeV/$C^2$) | 48 (0.0002GeV/$C^2$) |
| (26)Recoil $\pi^+\pi^-$ | 2.95~3.25 (GeV/$C^2$) | 3.095 (GeV/$C^2$) | 60 (0.0020GeV/$C^2$) |
| (27)$\pi^+\pi^-\pi^0$ | 0.65~0.90 (GeV/$C^2$) | 0.78 (GeV/$C^2$) | 35 (0.0020GeV/$C^2$) |
| (28)$p\pi^-$ | 1.100~1.130 (GeV/$C^2$) | 1.116 (GeV/$C^2$) | 310 (0.0002GeV/$C^2$) |
| (29)$\bar{p}\pi^+$ | 1.100~1.130 (GeV/$C^2$) | 1.116 (GeV/$C^2$) | 320 (0.0002GeV/$C^2$) |
| (30)$\gamma\gamma$ | 0.50~0.60 (GeV/$C^2$) | 0.546 (GeV/$C^2$) | 300 (0.0010GeV/$C^2$) |
| (31)$p\pi^-$ | 1.105~1.13 (GeV/$C^2$) | 1.116 (GeV/$C^2$) | 500 (0.00020GeV/$C^2$) |
| (32)$\bar{p}\pi^+$ | 1.105~1.13 (GeV/$C^2$) | 1.1165 (GeV/$C^2$) | 660 (0.00020GeV/$C^2$) |
| (33)Recoil $\pi^+\pi^-$ | 3.07~3.13 (GeV/$C^2$) | 3.098 (GeV/$C^2$) | 360 (0.00120GeV/$C^2$) |
| (34)$\pi^+\pi^-\pi^0$ | 0.65~0.90 (GeV/$C^2$) | 0.78 (GeV/$C^2$) | 210 (0.00208GeV/$C^2$) |
| (35)$p\pi^-$ | 1.06~1.16 (GeV/$C^2$) | 1.115 (GeV/$C^2$) | 6400 (0.00050GeV/$C^2$) |
| (36)$\bar{p}\pi^+$ | 1.06~1.16 (GeV/$C^2$) | 1.115 (GeV/$C^2$) | 6400 (0.00050GeV/$C^2$) |
| (37)$\gamma$ (coupled with $p\pi^-$) | 1.2~1.6 (GeV/$C^2$) | 1.36 (GeV/$C^2$) | 950 (0.00050GeV/$C^2$) |
| (38)$\gamma$ (coupled with $\bar{p}\pi^+$) | 1.2~1.6 (GeV/$C^2$) | 1.32 (GeV/$C^2$) | 950 (0.00050GeV/$C^2$) |

(1)(2) data is estimated according to the Fig 3.1 [32]; (3)(4) data is estimated according to the Fig 3.5 (b)(c) [32]; (5)(6) data is estimated according to the Fig 3.6 (b)(c) [32];(7) data is estimated according to the Fig 3.8(a) [32]; (8)(9) data is estimated according to the Fig 3.9(a)(b)[32]; (10) data is estimated according to the Fig 3-4(a) and Table 3-1 [33]; (11) data is estimated according to the Fig 3-3 [33]; (12) data is estimated according to the Fig 3.5 (a) [33]; (13) data is estimated according to the Fig 4.4 (Green data) [33]; (14) data is estimated according to the Fig 4.4 (Blue data) [33]; (15)(16)(17)(18)(19)(20)(21)(22)(23) data is estimated according to the Fig 3.3 [34]; (24)(25)(26)(27) data is estimated according to the Fig 3-3, 3-4, 3-8, 3-9, respectively [35]; (28)(29)(30) data is estimated according to the Fig 4-5, 4-6, 4-14, respectively [35];(31)(32)(33)(34) data is estimated according to the Fig 4.30, 4.31, 4.35, 4.38 [36]; (35)(36)(37)(38) data is estimated according to the Fig 5.6 (b)(c) and Fig 5.7 (a)(b) [36];

As shown in Table 3 (1)(2), BABAR collaboration team's findings show that the particle decaying events distribute along the mass range from 1.96 to 2.56 GeV/$C^2$, with the peak value at mass level of 2.11 GeV/$C^2$, whereas the BEIII collaboration team's results report the peak values at mass level of 2.38 GeV/$C^2$. However, the

events' amount at the peak observed by the BEIII collaboration team, 35 events (20 MeV/$C^2$), is apparently less than the BABAR collaboration team's event amount peak, which is 90 events (20 MeV/$C^2$).

From the Table 3 (3)(4), the result shows that the invariant mass spectrum range of $K^+K^-$ decaying process is between 1.0 and 1.8 at energy level of 2125 MeV, while the invariant mass spectrum range of $\pi^+\pi^-\gamma$ is significantly lower than it of $K^+K^-$, which falls between 0.3 and 1.1 at energy level of 2125 MeV. The peak events occur at mass level of 1.02 and 0.77 for $K^+K^-$ and $\pi^+\pi^-\gamma$, respectively, while the events' amount peak is 710 and 540 at the corresponding mass levels for $K^+K^-$ and $\pi^+\pi^-\gamma$, respectively.

Compared with particles of $K^+K^-$ and $\pi^+\pi^-\gamma$, the particle pair of $K^-\pi^+$ and $K^+\pi^-$ (Table 3(5)(6)) shows different invariant mass spectrum range in decaying process, from 0.62 to 1.20 (2125 MeV), and the peak events occur at mass level of 0.9 (2125 MeV) for both particles' state, which is lower than $K^+K^-$ but higher than $\pi^+\pi^-\gamma$.

Compared with particle state $\pi^+\pi^-\gamma$, particle state of $\pi^+\pi^-$ (Table 3(7)) distributes along similar mass range, from 0.28 to 1.05 (2125 MeV), and the peak events are detected at mass of 0.50 (2125 MeV), smaller than particle state $\pi^+\pi^-\gamma$, but the peak events' amount reaches the highest quantity of 820 among these particle states discussed in the same study.

At higher energy level of 3097 MeV (= 3.097 GeV), the particle state of Ø (Table 3(8)) is detected with mass range from 0.985 to 1.17, and the peak events is found at the mass level of 1.02. When the detectable energy unit is set to be 0.001 GeV/$C^2$, approximately 6400 events is found at the peak of events' quantity, significantly higher than the peak events at detectable energy units of both 0.003 GeV/$C^2$ and 0.004 GeV/$C^2$. Compared with $\pi^+\pi^-\gamma$ particle mass range (0.3 ~ 1.1) at energy level of 2125 MeV, higher mass range (0.9~1.1) is detected for the particles of $\pi^+\pi^-\gamma$ at energy level of 3097 MeV (Table 3(9)), with the peak events appearing at mass of 0.955 (3097 MeV). Approximately 2300 events of peak value are found for the particles of $\pi^+\pi^-\gamma$ at energy unit of 0.001 GeV/$C^2$, significantly higher than it at energy unit of 0.004 GeV/$C^2$ (540 events).

According to the Table 3(10~14), particle decaying chain of $\Psi(2S) \rightarrow \pi^0 h_c$ ($h_c \rightarrow 3(\pi^+\pi^-)$) has been studied with records of particle state: $\pi^+\pi^-$, Double Photons, $\pi^+\pi^-\pi^0$, $\gamma\gamma$. In order to make the data comparable with other experiment results, the units of data in Table 3(10~14) are converted into the same as the other data. Compared Table 3 (10) with (7) results, it is found that the mass range of state $\pi^+\pi^-$ in decaying chain of $\Psi(2S) \rightarrow \pi^0 h_c$ ($h_c \rightarrow 3(\pi^+\pi^-)$) is significantly larger than it at decaying chain of $e^+e^- \rightarrow$ Øη', reaching 1.0~3.5 mass level, which would be attributed to the higher energy level of 3686 MeV setting up for the decaying chain of $\Psi(2S) \rightarrow \pi^0 h_c$ ($h_c \rightarrow 3(\pi^+\pi^-)$).

Another state of particle $\pi^+\pi^-\pi^0$ is recorded in Table 3 (12), showing that the mass range is between 0.4 and 2.8 (3686 MeV) with peak events amount (4200) detected at mass level of 0.8. Particularly, the double photons' parameters are also analyzed in this study (Table 3(11)), with mass range from 0 to 0.16, and the peak events amount (8900) is found at the mass level of 0.13 with the energy level of 3686 MeV.

Particle state of γγ is studied on the decaying chains of both $J/\Psi\rightarrow\pi^0 3(\pi^+\pi^-)$ and $J/\Psi\rightarrow\gamma 3(\pi^+\pi^-)$, with the same mass range of 0.02~0.20 in both decaying chains. However, the peak events amount is found at higher mass level (0.18) in chain of $J/\Psi\rightarrow\gamma 3(\pi^+\pi^-)$ than it (0.135) in the chain of $J/\Psi\rightarrow\pi^0 3(\pi^+\pi^-)$, which is shown in Table 3 (13)(14). In order to be comparable with other research, the event data that have been screened in this study are not analyzed again in my article.

From Table 3(15~23), it can be seen that the mass range of these nine decaying pathways (approximately 1.835~1.885) is generally lower than it at the decaying pathways of both $J/\Psi\rightarrow\gamma\text{Ø}\eta$' and $J/\Psi\rightarrow\eta\text{Ø}\eta$'(approximately 1.96~2.56 in Table 3(1)(2)). The highest peak event amount is found at decaying pathway of $D^-\rightarrow K^+\pi^-\pi^-$ with 70 000 events that is reported at mass level of 1.87. Due to the finer detected unit of energy level (0.00025GeV/$C^2$), the overall peak event amount of these nine decaying pathways is significantly higher than it of other particle states. The peak events are found at approximately 1.865 mass level for decaying pathways of $\overline{D}\rightarrow K^+\pi^-$, $\overline{D}\rightarrow K^+\pi^-\pi^0$, $\overline{D}\rightarrow K^+\pi^-\pi^-\pi^+$, while peak event amount is detected at higher mass level of approximately 1.87 for decaying pathways of $D^-\rightarrow K^+\pi^-\pi^-$, $D^-\rightarrow K_s^0\pi^-$, $D^-\rightarrow K^+\pi^-\pi^-\pi^0$, $D^-\rightarrow K_s^0\pi^-\pi^0$, $D^-\rightarrow K_s^0\pi^-\pi^-\pi^+$, $D^-\rightarrow K^+K^-\pi^-$, respectively.

Compared Table 3(15) with Table 3(6), it is found that the final particle state ( $K^+\pi^-$) of decaying pathway $\overline{D}\rightarrow K^+\pi^-$ is the same as the particle state of Sun Yan-kun's study. From Table 3(24)~(27), different final particle states in the decaying pathway of $\Psi(3686)\rightarrow\Lambda\overline{\Lambda}\omega$ are characterized according to the mass range, mass level at peak events and peak event amount. The mass range for particle state of both $p\pi^-$ and $\bar{p}\pi^+$ is between 1.1000 and 1.1300, and their peak events are found at the mass level of approximately 1.1160 (GeV/$C^2$). It is found that the peak event amount of both $p\pi^-$ and $\bar{p}\pi^+$ is relatively fewer than other particle states, which is reported as only 45 and 48 for particle $p\pi^-$ and $\bar{p}\pi^+$ respectively at energy level unit of 0.0002GeV/$C^2$. The mass range for particle of recoil $\pi^+\pi^-$ becomes the highest one among these particle states, which is from 2.95 to 3.25, and its peak events are reported at the mass level of 3.095 with event amount of 60. Among these final particle states in the decaying pathway of $\Psi(3686)\rightarrow\Lambda\overline{\Lambda}\omega$, particle of $\pi^+\pi^-\pi^0$ falls in the lowest mass range, between 0.65 and 0.90, and its peak event amount is also the smallest one, 35 events.

Table 3 (28)~(30) lists the final particle states in the decaying pathway of $J/\Psi\rightarrow\Lambda\overline{\Lambda}\eta$. The mass range of both $p\pi^-$ and $\bar{p}\pi^+$ is the same as it in the decaying pathway of $\Psi(3686)\rightarrow\Lambda\overline{\Lambda}\omega$, but the peak events' amount becomes significantly higher, which is

310 and 320 for $p\pi^-$ and $\bar{p}\pi^+$ respectively, and this would be attributed to the finer energy unit detected (0.0002GeV/$C^2$) in the decaying pathway of $J/\Psi\rightarrow\Lambda\bar{\Lambda}\eta$.

Table 3 (31)~(34) further collects the collision data of final particle states in the decaying pathway of $\Psi(3686)\rightarrow\Lambda\bar{\Lambda}\omega$. Due to the same decaying pathway detected under the same experiment instruments, these data are comparable with previous experiment data shown in Table 3 (28)~(30). Obviously, compared with Table 3 (24)~(27), the events' amount is significantly increased by approximately ten times higher (such as 500 or 660) in the subsequent experiment as substantial supplement to the previous study (such as 45 or 48). However, the mass range of both $p\pi^-$ and $\bar{p}\pi^+$ remains unchanged in the subsequent experiment, from 1.105 to 1.13 in the same decaying pathway, and the peak events are reported at mass level of 1.116 (GeV/$C^2$), which is also similar to the previous study.

Table 3 (35)~(38) summarizes the later experiment data of final particle states in the decaying pathway of $J/\Psi\rightarrow\Lambda\bar{\Lambda}\eta$, which are comparable with Table 3 (28)~(30). The mass range and the mass level at which peak events appear for both $p\pi^-$ and $\bar{p}\pi^+$ are still at the same level as the previous study, but the peak events' amount are notably higher in the subsequent study, which reaches 6400 as compared to previous 320. It is found that the photon's mass range in the later experiment is apparently higher than the previous study, reaching 1.2~1.6 as comparison to the previous 0.50~0.60, and the peak quantity in event occurrence is also significantly increased to 950, compared with the previous one of 300.

**Table 4. Summary of particle's energy during particle decaying process.**

| Decaying process | Energy range | Energy at peak events | Peak Events |
|---|---|---|---|
| (1)$\gamma(e^+e^-\rightarrow \text{Ø}\eta')$ | 0.02 ~ 0.62 (2125 MeV) | 0.20 (2125 MeV) | 40 (0.020 GeV/C) |
| (2)$\gamma(J/\Psi\rightarrow\text{Ø}\eta')$ | 0.02 ~ 1.2 (3037 MeV) | 0.30 (3037 MeV) | 460 (0.010 GeV/C) |
| (3)$K^+K^-K^\pm$ | 1.5~3.5 (GeV) | 2.20 (GeV) | 125 (0.0263 GeV) |

(1)Data is estimated according to the Fig 3.8 (b)[32];(2) data is estimated according to the Fig 3.10 (d)[32];(3) data is estimated according to the Fig 3.11[37];

According to the Table 4 (1), the photon's energy of γ is recorded in the decaying process of $e^+e^-\rightarrow \text{Ø}\eta'$ with energy range between 0.02 and 0.62 (2125 MeV). The peak events appear at energy level of 0.20 (2125 MeV) with amount of 40 (0.020/GeV/C). In comparison, the photons' energy of γ is recorded at higher level of capturing energy (3037 MeV) with broader energy range from 0.02 to 1.2, as shown in Table 4 (2). When the detected energy unit is reduced from 0.020 to 0.010 GeV/C, the recorded peak events' amount is increased sharply from 40 to 460 events.

Table 4 (3) shows the total energy of final particle state of $K^+K^-K^\pm$, ranging from 1.5 to 3.5 (GeV), which falls in higher energy range than photon's energy in Table 4 (1)(2). The peak events are found at energy level of 2.20 (GeV), with amount of 125 detected at energy unit of 0.0263 (GeV).

**Table 5. Summary of particle's momentum during particle decaying process.**

| Decaying process | Momentum range | Momentum at peak events | Peak Events |
|---|---|---|---|
| (1) η' | 0.38~1.22 (3097 MeV) | 1.17 (3097 MeV) | 1550 (0.010 GeV/C) |
| (2) $\pi^-$ | 0.05~1.35 (3097 MeV) | 0.42 (3097 MeV) | 320 (0.010 GeV/C) |
| (3) $\pi^+$ | 0.05~1.35 (3097 MeV) | 0.50 (3097 MeV) | 320 (0.010 GeV/C) |
| (4) Ø | 0.4~1.22 (3097 MeV) | 1.18 (3097 MeV) | 1550 (0.010 GeV/C) |
| (5) $K^-$ | 0.36~0.82 (3097 MeV) | 0.64 (3097 MeV) | 560 (0.006 GeV/C) |
| (6) $K^+$ | 0.38~0.80 (3097 MeV) | 0.62 (3097 MeV) | 480 (0.006 GeV/C) |
| (7) $\pi^\pm$ | 0.1~0.7 (2125 MeV) | 0.3 (2125 MeV) | 160 (0.050 GeV/C) |
| (8) γ | 0~0.64 (2125 MeV) | 0.2 (2125 MeV) | 140 (0.090 GeV/C) |
| (9) $K^\pm$ | 0.02~0.35 (2125 MeV) | 0.23 (2125 MeV) | 280 (0.050 GeV/C) |
| (10) K1 | 0.1~1.5 (GeV/C) | 1.5 (GeV/C) | 650000 (0.0187 GeV) |
| (11) K2 | 0.1~1.5 (GeV/C) | 1.5 (GeV/C) | 650000 (0.0187 GeV) |
| (12) K3 | 0.1~1.5 (GeV/C) | 0.15 (GeV/C) | 2000000 (0.0187 GeV) |
| (13) μ | 0.1~1.5 (GeV/C) | 0.3 (GeV/C) | 1800000 (0.0187 GeV) |
| (14) K1 | 0.1~0.7 (GeV/C) | 0.65 (GeV/C) | 400 (0.0075 GeV) |
| (15) K2 | 0.1~0.7 (GeV/C) | 0.28 (GeV/C) | 480 (0.0075 GeV) |
| (16) K3 | 0.1~0.7 (GeV/C) | 0.16 (GeV/C) | 1700 (0.0075 GeV) |
| (17) μ | 0.5~1.5 (GeV/C) | 0.70 (GeV/C) | 2900 (0.0187 GeV) |
| (18) K1 | 0.1~0.7 (GeV/C) | 0.67 (GeV/C) | 190 (0.0075 GeV) |

| | | | |
|---|---|---|---|
| (19) K2 | 0.1~0.7 (GeV/C) | 0.27 (GeV/C) | 170 (0.0075 GeV) |
| (20) K3 | 0.1~0.7 (GeV/C) | 0.22 (GeV/C) | 290 (0.0075 GeV) |
| (21) μ | 0.5~1.5 (GeV/C) | 0.70 (GeV/C) | 700 (0.0187 GeV) |
| (22) K1 | 0.1~0.7 (GeV/C) | 0.35 (GeV/C) | 9 (0.0075 GeV) |
| (23) K2 | 0.1~0.7 (GeV/C) | 0.35 (GeV/C) | 5.5 (0.0075 GeV) |
| (24) K3 | 0.1~0.7 (GeV/C) | 0.22 (GeV/C) | 5.5 (0.0075 GeV) |
| (25) μ | 0.5~1.5 (GeV/C) | 0.75 (GeV/C) | 9 (0.0187 GeV) |

(1)data is estimated according to the Fig 3.10 (a)[32]; (2) data is estimated according to the Fig 3.10 (b)[32]; (3) data is estimated according to the Fig 3.10 (c)[32]; (4) data is estimated according to the Fig 3.10 (e)[32]; (5) data is estimated according to the Fig 3.10 (f)[32]; (6) data is estimated according to the Fig 3.10 (g)[32]; (7) data is estimated according to the Fig 3.15 (a)[32]; (8) data is estimated according to the Fig 3.15 (b)[32]; (9) data is estimated according to the Fig 3.15 (c)[32]; (10)(11)(12)(13) data is estimated according to the Fig 3.2 [37]; (14)(15)(16)(17) data is estimated according to the Fig 3.4 [37]; (18)(19)(20)(21) data is estimated according to the Fig 3.6 [37]; (22)(23)(24)(25) data is estimated according to the Fig 3.12 [37];

The particle momentum has been recorded at energy level of 3097 MeV, with momentum range of 0.38~1.22, 0.05~1.35, 0.05~1.35, 0.4~1.22, 0.36~0.82 and 0.38~0.80 for particle state of η', $\pi^-$, $\pi^+$, Ø, $K^-$ and $K^+$, respectively (Table 6 (1)~(6)). The momentum at peak events for η' and Ø is the highest among these particle states, found at 1.17 and 1.18 level respectively. Correspondingly, the peak events' amount is also the highest for particles of η' and Ø, with approximately 1550 events for both of them, while the other particles' peak event amount is 320, 320, 560, 480 events for $\pi^-$, $\pi^+$, $K^-$, $K^+$ respectively, found at momentum level of 0.42, 0.50, 0.64 and 0.62 correspondingly.

The particle momentum is also recorded at lower energy level of 2125 MeV for particle state of $\pi^{\pm}$, γ, $K^{\pm}$(Table 5 (7)~(9)). The momentum range of particle state of both $\pi^{\pm}$ and $K^{\pm}$ is generally less than it at higher energy level of 3097 MeV, which falls in 0.1~0.7 and 0.02~0.35 respectively. The peak events is found at momentum level of 0.3 and 0.23 for $\pi^{\pm}$ and $K^{\pm}$ respectively, with peak amount of 160 and 280 correspondingly. Particle state of γ is recorded at energy level of 2125 MeV only, without records at energy level of 3097 MeV. Its momentum ranges from 0 to 0.64 (2125 MeV), with peak events occurring at momentum level of 0.20, and the peak event amount is 140 at the detected energy unit of 0.090 GeV/C that is the highest one among these particle states, consequently resulting in the least amount of peak events.

Particle momentum of four states is recorded in the decaying pathway of $\tau^+\tau^- \rightarrow K^+K^-K^{\pm}\mu^{\pm}\mu_{\mu}$ $(\bar{\mu}_{\mu})\bar{\mu}_T\mu_T$ at energy level of 3686 MeV. To screen the event data, the criterion of $\chi_{\mu}$ (as introduced in equation 67) is adopted to treat the raw collision data. The conditions to screen the data scope for particle momentum calculation are imposed step by step, so the analyzed events' amount is decreased correspondingly from 650000 to 5.5 with increasingly imposed conditions. When $\chi_{\mu}$ falls in the range of [-2, 2], particle momentum range is between 0.1 and 1.5 for all the four states, including K1, K2, K3 and μ (Table 5(10)~(13)). Event amount increases with the increasing particle momentum for K1 and K2, so the peak events are also found at peak momentum level, 1.5 for the both. However, for the particle state K3, the peak events are reported at 0.15 momentum level; When the screening criterion of the joint distribution between the incident depth and incident momentum of μ particle detector is further imposed, the calculated momentum range is decreased to 0.1~0.7 for K1, K2, K3, and the peak event is reported at momentum level of 0.65, 0.28, 0.16 respectively (Table 5(14)~(17)). Final state of μ particle shows the momentum range of 0.5~1.5 with peak event found at 0.70 momentum level; When the $\chi_{\mu}$ criterion is applied on the K1, K2, K3 separately, both the momentum range and the momentum level of peak event appearing are still similar to it before application of this screening criterion, although the events' amount is decreased sharply due to this screening criterion (Table 5(18)~(21)); Finally, the screening criterion of total particle energy E(KKK) is imposed on the event data to further refine the data, the momentum range still remains similar, but the momentum level where the peak events are found is lowered, which is 0.35, 0.35, 0.22 for K1, K2, K3 respectively (Table 5(22)~(25)).

### 8.3.Original discussion

Comprehensively analyzed from the Table 3, some of the final state of particles for the hadronic decaying characteristics of D meson may be the mixture state of other research. For example, compared Table 3(20) with Table 3(6)(12), the final particle state of $K^+\pi^-\pi^-\pi^0$ may be the mixture state of both $K^+\pi^-$ and $\pi^+\pi^-\pi^0$; Compared Table 3(23) with Table 3(3)(6), the final particle state of $K^+K^-\pi^-$ may be the mixture state of both $K^+K^-$ and $K^+\pi^-$; According to the results of Table 3(3)~(6), it can be deduced that the particle state of $K^-\pi^+$ and $K^+\pi^-$ is the crossing particle pairs for $K^+K^-$ and $\pi^+\pi^-\gamma$, which may be the metastable composite.

It can be seen from the above Tables that the more precision in detected energy unit results in higher amount of peak events identified, and this would reflect that the various final-state particle sizes that are generated by the particle collision motion are finer than the precision set up by the instrument, so in theory the final-state particle size may be infinitely partitioned into smaller one by the particle collision with higher energy level. This means that exploring finer particles by investing higher energy particle collision equipment may be meaningless.

Table 4 analyzes the energy of neutral particles: photons' energy. However, my article argues that these neutral particles detected in particle collision experiment may not be

the photons, but may be the particles partitioned from the neutrons. The energy generation mechanism by these neutral particles (including photons) is explained by the Figure 2 in above section.

Figure 4 of this article has illustrated that the measurable mass of elementary particles is not constant in the wave-like acceleration motion, which is further supported by the mass data in Table 3: for any of particle states that are identified by equipment, the mass of each particle state is varying over a mass range. However, the frequency of particle mass occurrence at a specific value can be deduced according to the Table 3. For example, from Table 3 (10) results, the peak events' amount of particle $\pi^+\pi^-$ occurs at mass level of 3.10 (3686 MeV), indicating that mass level of 3.10 would show the highest frequency of occurrences among the overall mass range from 1.0 to 3.5. Therefore other particles' specific mass occurrence frequency can be deduced in the same way. Similarly, the energy and momentum of each particle state is also not constant as summarized in Table 4 and Table 5 respectively, which provides the experimental argument to modify the variables of particle energy and momentum in Schrodinger equation, and this will be further discussed in the next section of this article.

By comparing the results within Table 3, it is found that the peak events of particle $\pi^+\pi^-$ occur at the highest mass level of 3.10 (3686 MeV), while double photons' peak events is recorded at the lowest mass level of 0.13 (3686 MeV), which may indicate that the resonance state of particle $\pi^+\pi^-$ appears at the highest mass level among all the particle states summarized in Table 3, and the resonance state of double photons happens at the lowest mass level.

This article has newly proposed the theoretical equation 17 ($P1 = a \times E_e/\lambda$) and equation 18 ($P2 = b \times E_m \times c$) in above section, which may be feasibly re-analyzed according to the parameters of particle collision data: $E_e$ data can be obtained by the MDC instrument which records the electric charges of particles; $E_m$ data can be derived by the EMC instrument part that measures the energy of both charged particles and neutral particles; $\lambda$ and c represent the electromagnetic wave frequency generated by the beam of particles and velocity of particle motion, respectively, which can be recorded by EMC, MDC and TOF instruments; finally each vector momentum (P1 and P2) can be calculated correspondingly, in comparison to the momentum measured by the superconducting magnet in the particle collision experiment.

In summary, the previous case studies have not characterized the above Table data in more details, which have been filled in by this section, and my article has attempted to re-analyze the particle collision data in a new method, with emphasis on the relationship among particle energy, mass and momentum.

## 9. Quantum wave experiment and modeling

The limitation and uncertainty of linear formula of Schrodinger equation have been

pointed out by my another quantum chemistry article [38], especially when this Schrodinger equation is applied on the energy level transition of elementary particles, because the transition motion between different energy orbitals is believed as NOT the linear math model, but is the model of incontinuous jumping points. Consequently, this section will focus on the quantum wave experiment findings' characterization, rather than the theoretical equations' demonstration of quantum chemistry which is less meaningful considered by me.

### 9.1.Case study

One of common technologies is to utilize the nonlinear crystals to prepare probabilistic single-photon sources in the process of spontaneous parametric down conversion (SPDC), in which high-energy pump photons are spontaneously converted into signal photons and idle frequency photons with a very low probability, so a pair of associated photons is produced for the spectral analysis. Both energy and momentum conservation Laws are approximately applied to this photon conversion process, which are expressed as [39]:

$$\omega_p = \omega_s + \omega_i \qquad \text{equation 68}$$

$$\overrightarrow{K_p} = \overrightarrow{Ks} + \overrightarrow{Ki} \qquad \text{equation 69}$$

Where $\omega_p$, $\omega_s$, $\omega_i$ are the angular frequencies of pump light, signal light and idle frequency light respectively; $\overrightarrow{K_p}$, $\overrightarrow{Ks}$, $\overrightarrow{Ki}$ are the wave vector of pump light, signal light and idle frequency light respectively [39].

According to the polarization characteristics among pump's photon, signal photon and idle photon, the SPDC is classified into three types: when three photons possess identical polarization, it is classified as Type 0; If the signal photon and idle photon have the same polarization but are orthogonal to the pump's polarization, it is defined as Type I; When the signal photon and idle photon exhibit perpendicular polarization, it corresponds to Type II. Furthermore, based on light wave propagation direction, SPDC can be categorized into collinear or non-collinear, and there is also another wavelength-dependent classification method, including degenerate and non-degenerate types. Degenerate waves possess the same wave length or frequency with different fields, whereas non-degenerate waves show different wave length or frequency. Under the degenerate temperature, degenerate waves are produced so that different wave functions can be superimposition [39].

Cheng Long (2021) adopted a kind of dynamics approach to model and investigate electron diffraction in TEM, including both parallel beam diffraction lattices and convergent beam electron diffraction (CBED). For parallel electron beams, multiple crystal orientation of diffraction lattices were compared among them by using kinematic models. Additionally, the scenarios beyond dynamics models were also

discussed in research, specifically including variation of intensities with the changing sample thickness in both zeroth-order beam and diffraction beam, and the variation curves for different crystal orientations were correspondingly drawn [40].

### 9.2. Results and description

**Table 6. Spectral characteristics varying with different temperature among different materials types.**

| Temperature (℃) | Light photon type | Center Wavelength (nm) | Materials type (pump light wavelength) |
|---|---|---|---|
| (1)30 | Signal | 786 | Type-II(404.3 nm) |
| (2)30 | Idler | 830 | Type-II(404.3 nm) |
| (3)50 | Signal | 790 | Type-II(404.3 nm) |
| (4)50 | Idler | 826 | Type-II(404.3 nm) |
| (5)100 | Signal | 804 | Type-II(404.3 nm) |
| (6)100 | Idler | 816 | Type-II(404.3 nm) |
| (7)126.8 | Signal | 810 | Type-II(404.3 nm) |
| (8)126.8 | Idler | 810 | Type-II(404.3 nm) |
| (9)150 | Signal | 816 | Type-II(404.3 nm) |
| (10)150 | Idler | 804 | Type-II(404.3 nm) |
| (11)50 | Signal | 810 | Type-I(404.3 nm) |
| (12)50 | Idler | 810 | Type-I(404.3 nm) |
| (13)57.2 | Signal | 814 | Type-I(404.3 nm) |
| (14)57.2 | Idler | 814 | Type-I(404.3 nm) |
| (15)70 | Signal | 880 | Type-I(404.3 nm) |
| (16)70 | Idler | 730 | Type-I(404.3 nm) |
| (17)80 | Signal | 890 | Type-I(404.3 nm) |
| (18)80 | Idler | 720 | Type-I(404.3 nm) |
| (19)90 | Signal | 920 | Type-I(404.3 nm) |
| (20)90 | Idler | 680 | Type-I(404.3 nm) |
| (21)40 | Signal | 820 | Type-0 (408.8 nm) |
| (22)40 | Idler | 820 | Type-0 (408.8 nm) |
| (23)58.4 | Signal | 825 | Type-0 (408.8 nm) |
| (24)58.4 | Idler | 825 | Type-0 (408.8 nm) |
| (25)80 | Signal | 880 | Type-0 (408.8 nm) |
| (26)80 | Idler | 750 | Type-0 (408.8 nm) |
| (27)100 | Signal | 900 | Type-0 (408.8 nm) |
| (28)100 | Idler | 720 | Type-0 (408.8 nm) |
| (29)120 | Signal | 925 | Type-0 (408.8 nm) |
| (30)120 | Idler | 675 | Type-0 (408.8 nm) |

| | | | |
|---|---|---|---|
| (31)30 | Signal | 630 | Type-II(315 nm) |
| (32)30 | Idler | 639 | Type-II(315 nm) |
| (33)60 | Signal | 634 | Type-II(315 nm) |
| (34)60 | Idler | 634 | Type-II(315 nm) |
| (35)62.8 | Signal | 633 | Type-II(315 nm) |
| (36)62.8 | Idler | 633 | Type-II(315 nm) |
| (37)120 | Signal | 645 | Type-II(315 nm) |
| (38)120 | Idler | 625 | Type-II(315 nm) |
| (39)150 | Signal | 650 | Type-II(315 nm) |
| (40)150 | Idler | 620 | Type-II(315 nm) |
| (41)Not list | Pump | 405.2 | Combination of materials with controllable transformation process |
| (42)28.5 | Degenerate waves | 810.1 | |

Data (1)~(10) are estimated according to Fig 3-3 (e)[39]; Data (11)~(20) are estimated according to Fig 3-3 (f)[39]; Data (21)~(30) are estimated according to Fig 3-3 (g) [39]; Data (31)~(40) are estimated according to Fig 3-3 (h) [39]; Data (41)(42) are estimated according to Fig 3-5 (a)(b) respectively [39];

The light wave intensity's distribution along different wavelengths generally appears to be the shape of normal distribution rate, and the wavelength at which peak intensity occurs is named as the center wavelength [39]. Table 6 (1)~(10) summarizes both signal and idler light waves' center wavelengths that vary with the changing temperature on Type-II (404.3 nm) material tested in this experiment, and it is found that the signal wave's center wavelengths are positively correlated with the increasing temperature from 30 to 150 ℃, whereas the idler light wave shows negative correlation between center wavelength and increased temperature. When the tested temperature ascends from 30 to 150 ℃, the center wavelengths of signal wave increase from 786 to 816 nm, but the center wavelengths of idler wave decrease from 830 to 804 nm. However, both signal wave and idler wave show the same level of center wavelength at the temperature of 126.8 ℃, called as degenerate temperature, at which both signal and idler waves turn to be the degenerate waves.

The correlations between center wavelength and tested temperature on materials Type-I (404.3 nm) differs from the Type-II (404.3 nm). According to the Table 6 (11)~(20), when materials temperature ascends from 50 to 57.2℃, the center wavelength does not change significantly and 57.2℃ is the critical level of materials temperature, degenerate temperature, below which both signal wave and idler wave possess the same range of center wavelength so that double waves' state (such as intensity and field) can be superimposition as the quantum state. However, when the tested temperature exceeds 57.2℃, the signal center wavelength is positively related with increased temperature, while the idler center wavelength is negatively correlated.

The spectral characteristics of materials Type-0 (408.8 nm) is similar to the materials Type-I (404.3 nm), summarized in Table 6 (21)~(30), whose center wavelength does

not vary apparently when materials temperature increases from 40℃ to the degenerate temperature of 58.4℃. When the tested temperature exceeds this degenerate temperature, the signal center wavelength increases from 880nm to 925nm with the ascending temperature, but the idler center wavelength decreases from 750nm to 675nm with the increased temperature. Consequently, both materials Type-I (404.3 nm) and Type-0 (408.8 nm) do not only show the similar level of degenerate temperature, but also reveal similar correlations between tested temperature and center wavelengths, nevertheless both of which differ from the spectral characteristics of materials Type-II (404.3 nm).

Compared with the first three types of materials, the spectral characteristics of Type-II (315 nm) displays distinct difference (as summarized in Table 6(31)~(40)): when the tested temperature ascends from 30℃ to 150℃, the signal center wavelength increases from 630nm to 650nm, whereas the idler center wavelength decreases from 639nm to 620nm. The correlation trend lines of Type-II (315 nm) are similar to the Type-II (404.3 nm) material, but the degenerated temperature of Type-II(315 nm), 62.8℃, is apparently lower than it of Type-II (404.3 nm), which means that the decreased wavelength of pump light (from 404.3 nm to 315 nm) significantly reduces the degenerated temperature of materials (from 126.8℃ to 62.8℃).

An improved interferometer of HOM by a combination of materials with controllable transformation process is designed in this research, and the spectral characteristics of this designed HOM is summarized in Table 6(41)(42). The tested pump light's center wavelength is 405.2nm, and the center wavelength of degenerated waves for both signal and idler waves is 810.1nm under the degenerate temperature of 28.5℃, which is the lowest degenerate temperature level among all the materials types.

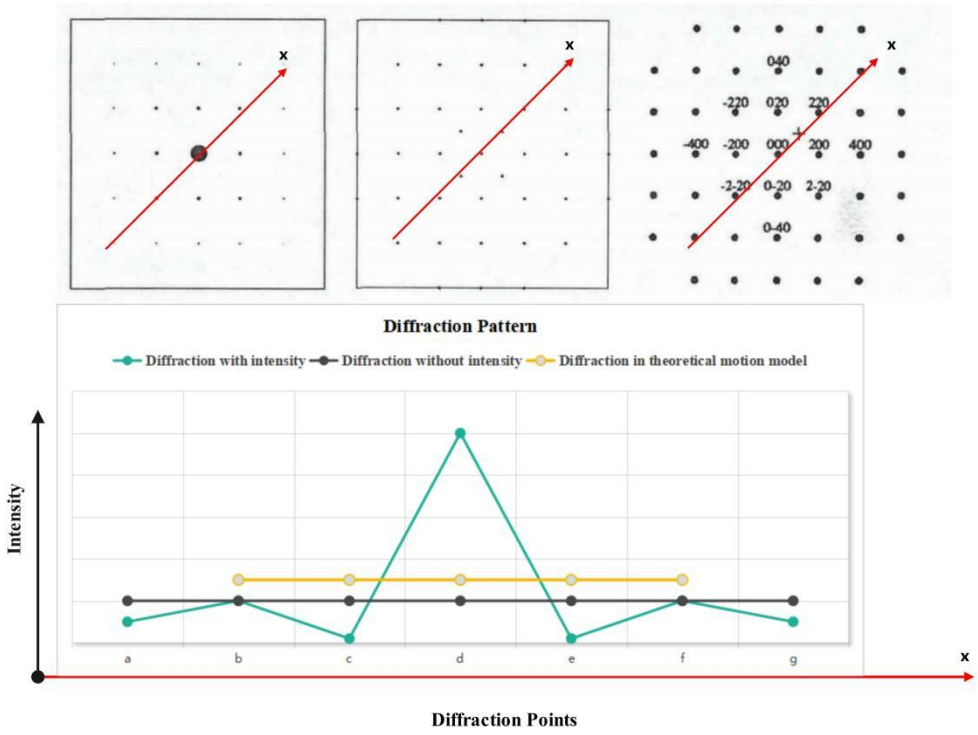



**Figure 7. Diffraction pattern of parallel illumination of electron beams through the Au metal plate of face-centered cubic structure with [001] crystal orientation.** Data Source: data of Figure 7 (down graph) is estimated according to the Fig 3.3 (a) [40]; Please note: the intensity data (down graph) is estimated according to the relative size of diffraction points, and the value of intensity in Figure 7 is the relative value only. The diffraction pattern (up graph) of Figure 7 is under the conditions that the acceleration voltage is 200 kV and the sample thickness of Au metal plate is 100 nm [40].

The upper figure of Figure 7 is modified on the basis of case study, and the red arrow is additionally drawn to indicate the x axis, along which the diffraction points are represented by a, b, c, d, e, f, g in the bottom figure of Figure 7, respectively. There are three diffraction patterns compared by Figure 7, including diffraction with intensity value (indicated by green colour), diffraction without intensity value (indicated by dark colour), diffraction in theoretical motion model (indicated by yellow colour). Along x axis, the diffraction points with intensity value at ‘c’ and ‘e’ show very weak intensity, which can be hardly observed by eyes in the diffraction graph, whereas the middle point ‘d’ between ‘c’ and ‘e’ displays the highest diffraction intensity among all the diffraction points. In comparison between diffraction without intensity value and diffraction in theoretical motion models, the diffraction points ‘a’ and ‘g’ have not been simulated to appear by the theoretical motion models.

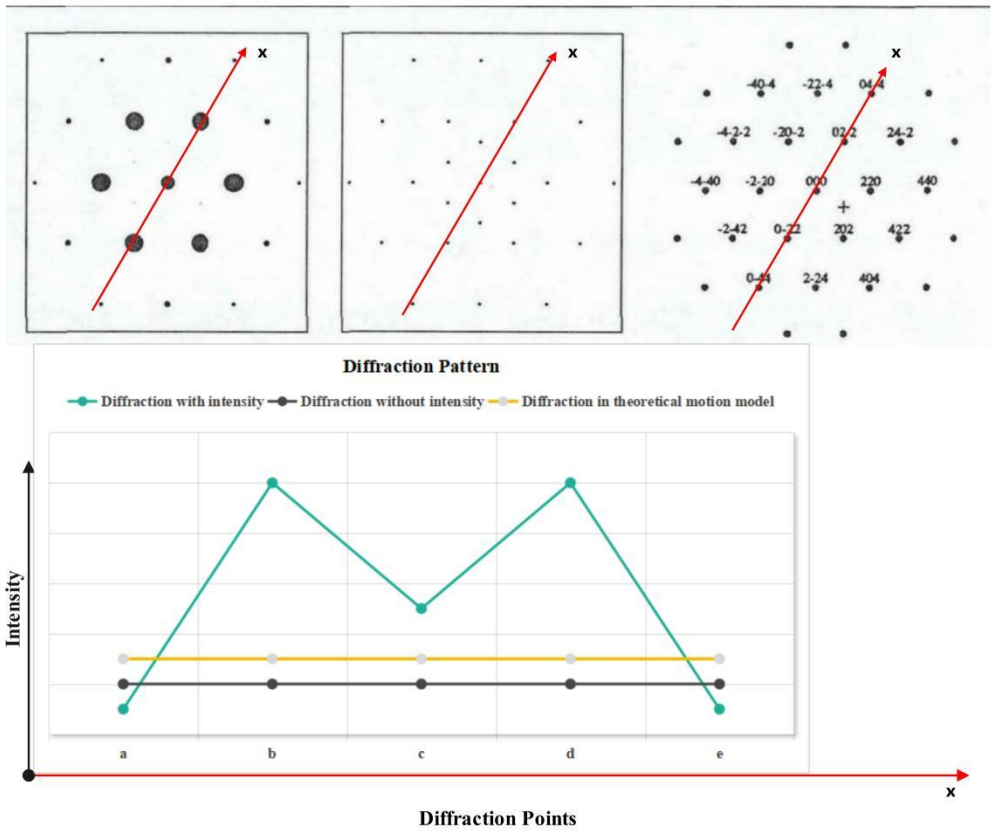



**Figure 8. Diffraction pattern of parallel illumination of electron beams through the Au metal plate of face-centered cubic structure with [-111] crystal orientation.** Data Source: data of Figure 8 (down graph) is estimated according to the Fig 3.3 (c) [40]; Please note: the intensity data (down graph) is estimated according to the relative size of diffraction points, and the value of intensity in Figure 8 is the relative value only. The diffraction pattern (up graph) of Figure 8 is under the conditions that the acceleration voltage is 200 kV and the sample thickness of Au metal plate is 100 nm [40].

Similar to Figure 7, a red line is drawn in the diffraction graph (up part of Figure 8) of case study as the x axis, along which each diffraction point is shown to reflect the diffraction pattern (down part of Figure 8). Differed from the Figure 7, there are totally two peak diffraction points on the x axis rather than one peak diffraction point like Figure 7, and the peak diffraction points include both 'b' and 'd', between which there is a weaker diffraction point 'c'. This finding of Figure 8 means that the center diffraction point is not the peak intensity point but its adjacent points are the peaks, while the center diffraction point is definitely the peak intensity point in Figure 7. It is reported that the theoretical motion models have accurately simulated all the diffraction points along x axis in Figure 8.

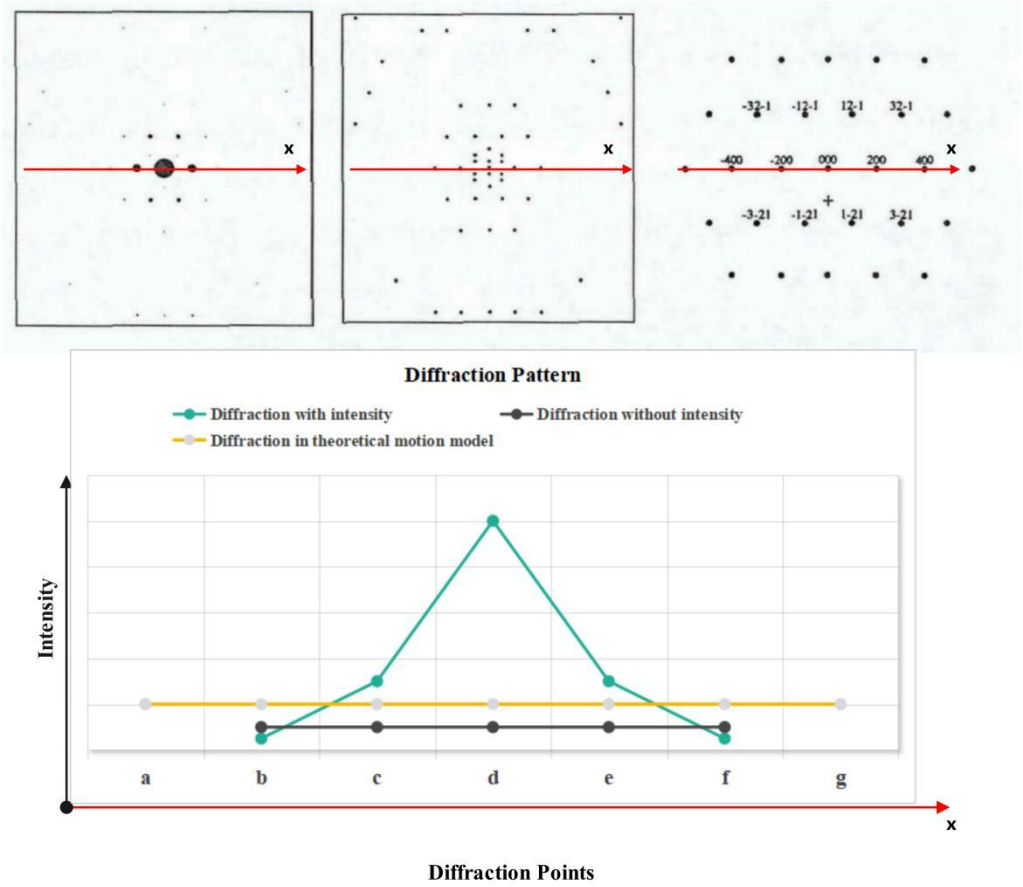



**Figure 9. Diffraction pattern of parallel illumination of electron beams through the Mo metal plate of face-centered cubic structure with [012] crystal orientation.** Data Source: data of Figure 9 (down graph) is estimated according to the Fig 3.6 (d) [40]; Please note: the intensity data (down graph) is estimated according to the relative size of diffraction points, and the value of intensity in Figure 9 is the relative value only. The diffraction pattern (up graph) of Figure 9 is under the conditions that the acceleration voltage is 200 kV and the sample thickness of Mo metal plate is 100 nm [40].

In Figure 9, the highest intensity of diffraction point is found in the center point of 'd', and the intensity of diffraction points gradually decreases on the both sides of center point 'd'. In comparison between diffraction without intensity (dark line) and diffraction in theoretical motion models (yellow line), the theoretical motion models simulate more diffraction points along x axis, including point 'a' and 'g', but these two diffraction points are not shown in the diffraction graph calculated by empirical dynamics model.

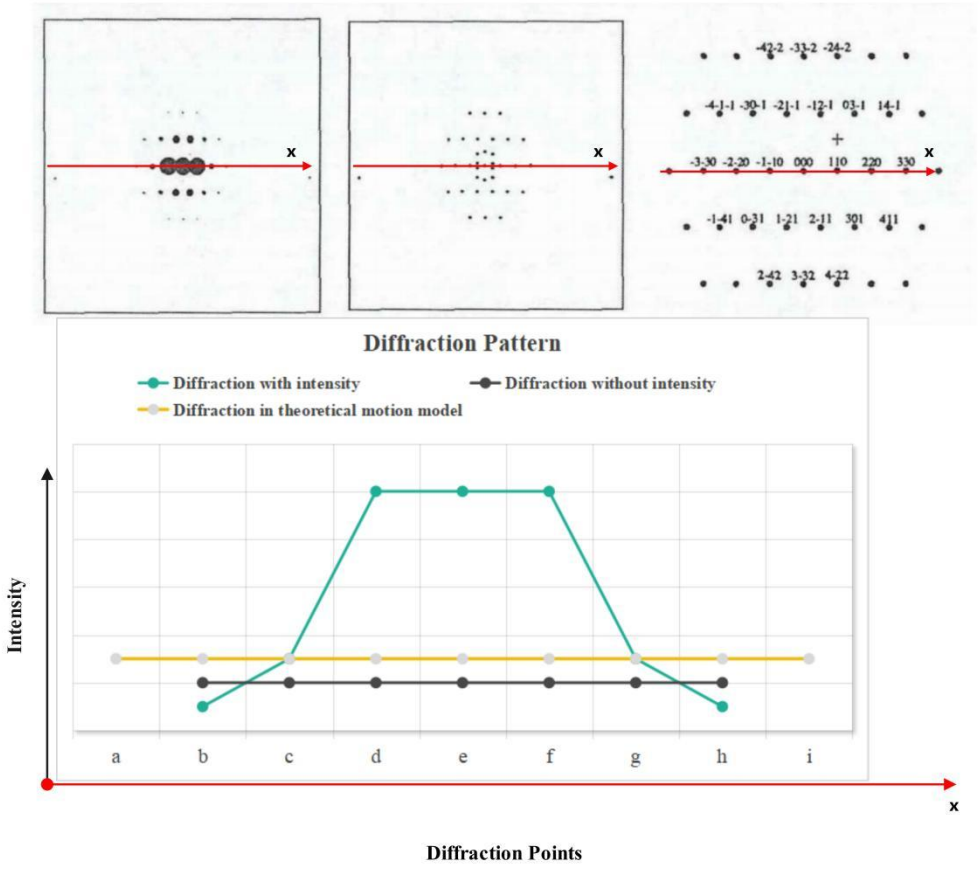



**Figure 10. Diffraction pattern of parallel illumination of electron beams through the Mo metal plate of face-centered cubic structure with [-113] crystal orientation.** Data Source: data of Figure 10 (down graph) is estimated according to the Fig 3.7 (d) [40]; Please note: the intensity data (down graph) is estimated according to the relative size of diffraction points, and the value of intensity in Figure 10 is the relative value only. The diffraction pattern (up graph) of Figure 10 is under the conditions that the acceleration voltage is 200 kV and the sample thickness of Mo metal plate is 100 nm [40].

As shown in Figure 10, there are three peaks appearing in the middle of diffraction line with intensity (green line), while the intensity of other diffraction points gradually decreases on both sides of diffraction peaks. Compared with diffraction without intensity (dark line), the diffraction in theoretical motion models (yellow line) simulates more diffraction points of 'a' and 'i' along x axis, which means that the theoretical motion models result in the bias of diffraction point distribution.

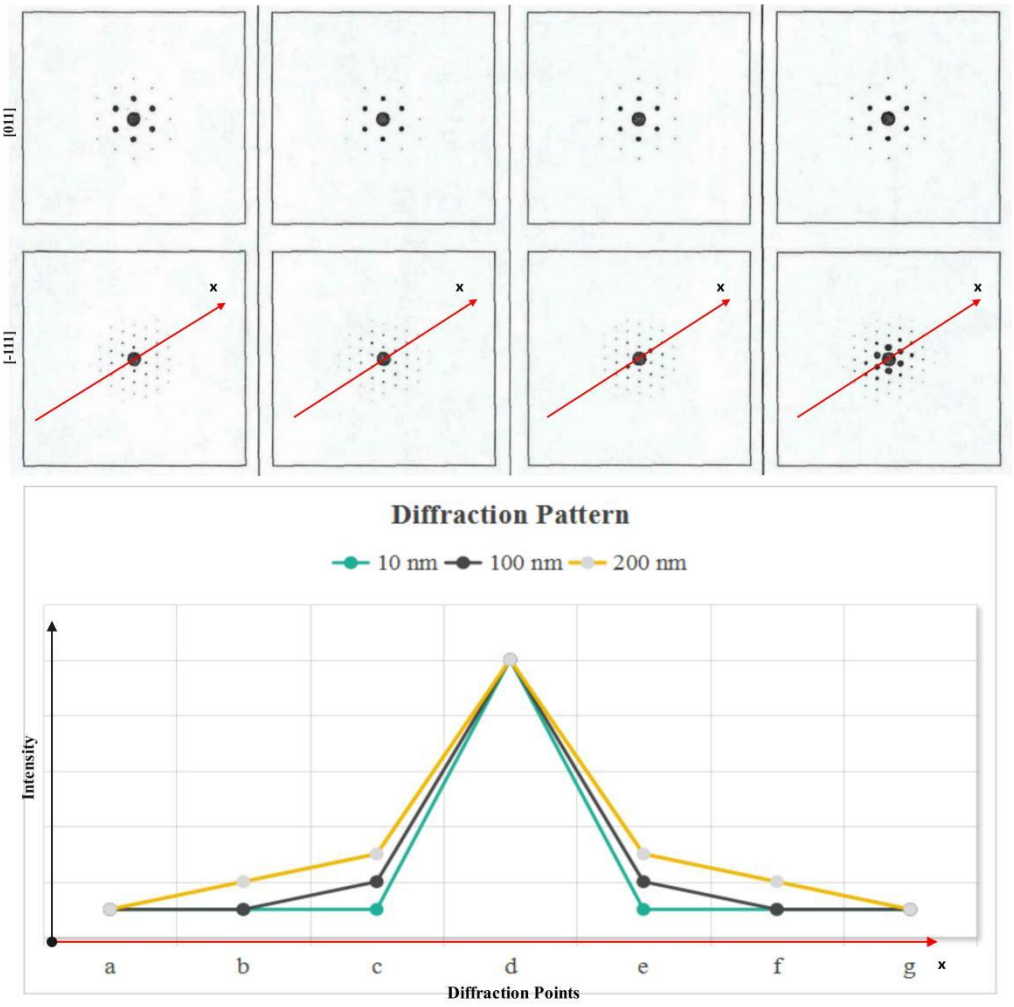



**Figure 11. Diffraction patterns of parallel illumination of electron beams through the Au metal plate of face-centered cubic structure with [011] and [-111] crystal orientation by using different sample thickness.** Data Source: data of Figure 11 (down graph) is estimated according to the Fig 3.9 for [-111] crystal orientation only; Please note: the intensity data is estimated according to the relative size of diffraction points, and the value of intensity in Figure 11 (down graph) is the relative value only. The diffraction pattern (up graph) of Figure 11 is under the conditions that the acceleration voltage is 200 kV and the sample thickness of Au metal plate is 10 nm, 50 nm, 100 nm, 200 nm from left to right, respectively [40].

The up graph of Figure 11 selects different diffraction patterns of two crystal orientations ([011] and [-111]) to compare, and it is found that the intensity of diffraction points does not vary significantly with the increased sample thickness for the [011] crystal orientation, whereas the sample thickness apparently influences the intensity of diffraction points for the [-111] crystal orientation. To further analyze the effects of sample thickness on the diffraction point intensity for the [-111] crystal orientation, the red arrows are drawn to indicate the x axis, along which each

diffraction point is shown in the ‘a’, ‘b’, ‘c’, ‘d’, ‘e’, ‘f’, ‘g’ points. As can be seen from the down graph of Figure 11, the peak intensity point is ‘d’, which is not apparently influenced by the increased sample thickness, but its adjacent diffraction points of both ‘c’ and ‘e’ gradually increase the intensity with the ascending sample thickness.

Case study also reported that inelastic scattering did not apparently change the shape of the diffraction pattern in principle, but resulted in great influence on the intensity of the diffraction beams. Especially with the increase of the sample thickness, the overall intensity of the wave function significantly varied by the inelastic scattering [40]. During particle interaction process, elastic scattering means that particle beams retain their original energy in total, whereas inelastic scattering usually may cause the particles to lose part of its energy during interaction process [41].

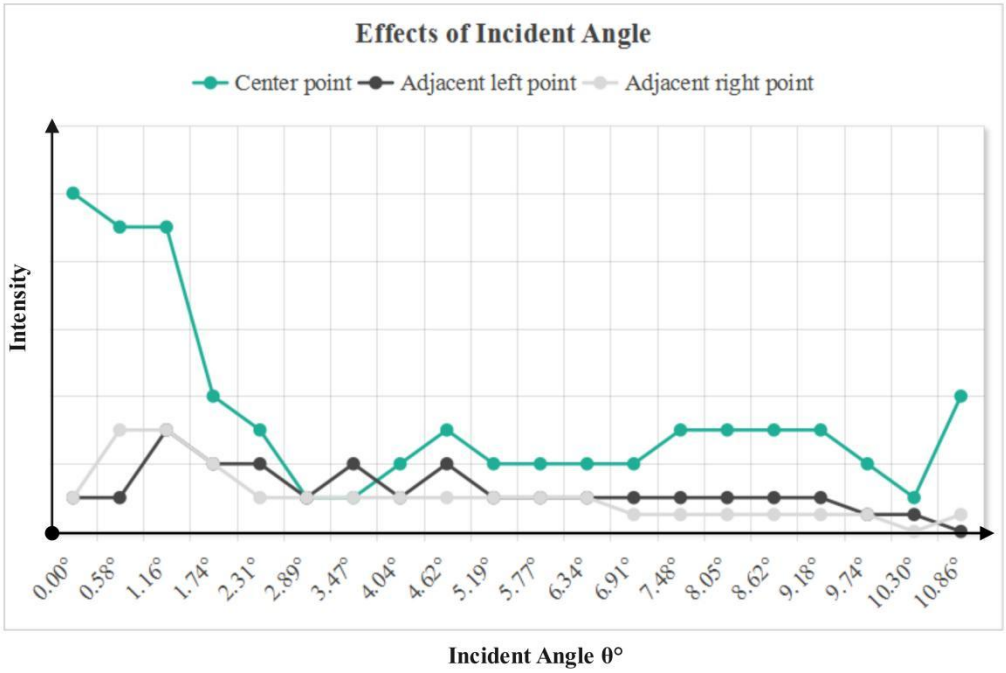



**Figure 12. Testing the effects of incident angle (θ°) on the intensity of diffraction points.** The green points indicate the diffraction point at the center point; the dark points indicate its adjacent diffraction point at the left; the blue points indicate its adjacent diffraction point at the right. The diffraction pattern of Figure 12 is under the conditions that the acceleration voltage is 200 kV and the sample thickness of Au metal plate is 10 nm, with crystal orientation of [001]. Data Source: data of Figure 12 is estimated according to the Fig 3.17 [40]; Please note: the intensity data is estimated according to the relative size of diffraction points, and the value of intensity in Figure 12 is the relative value only.

As can be seen from Figure 12, the intensity of each diffraction point varies with the change of incident angles, but the variation rate differs among these diffraction points. For the diffraction point at the center, incident angle results in the most significant

effects on the intensity among all the diffraction points, whereas the diffraction points adjacent the center point show less influence caused by incident angle on the intensity. When the incident angles change from 1.16° to 2.89°, the intensity of three representative diffraction points all shows decreasing trends; when the incident angles increase from 10.30° to 10.86°, the intensity of diffraction point at the center apparently increases in response.

### 9.3.Original discussion

Table 6 and the corresponding description of my article emphasizes on the correlation between tested materials temperature and center wavelength, aiming to evaluate the temperature effects on the materials' spectral characteristics, which has not been covered in the previous case study. It is concluded that generally the signal waves' center wavelength increases with the increasing materials temperature, while the center wavelength of idler waves descends with the increasing temperature.

Under degenerate temperature of materials, both signal and idler waves' center wavelengths display at the same level, so interference of light waves may occur and superimposition of different wave functions is applicable, which turns to be the 'quantum superposition' state as discussed above in the 4.9 section of my article. Consequently this degenerate temperature should be the essential requirement for the application of tested materials on the spectral analysis by using interferometer. It is to compare the advantages/disadvantages of different degenerate temperatures next: it is found that the highest degenerate temperature is reported on the materials Type-II(404.3 nm) among all the materials types, 126.8℃, and such high temperature requirement may accelerate the aging of tested materials if the materials testing is required frequently; then it is to decrease the degenerate temperature by refining the pump light's center wavelength (or increasing its frequency) from 404.3nm to 315nm, and the corresponding degenerate temperature is reduced to 62.8℃, but the increased intensity of pump light waves should significantly result in higher energy consumption by using interferometer; the third method is to design an improved interferometer of HOM by a combination of materials with controllable transformation process, which reduces the degenerate temperature to 28.5℃, and this routine temperature should be the acceptable one for the interferometer application in practice, due to its convenience and energy-saving, although this improvement may cause higher cost of spectral materials. Consequently, my article has characterized the advantages/disadvantages among different spectral materials, which should become the helpful complement to the previous case study.

Discussed in the 4.9 section of this article, the 'quantum superposition' state of elementary particle waves is defined as the condition that superimposition of different wave functions is applied due to the interference of different waves. This 'quantum superposition' condition becomes the prerequisite of spectral analysis by using interferometer in the case study: both signal and idler waves' frequency (or center wavelength) at the peak intensity must be at the same level, which can be achieved by

adjusting the temperature of spectral materials to the suitable degenerate one; Similarly, my another article also proposed that "the most efficient 'heating' process is the electromagnetic waves from external thermal sources, which have the same frequency as the electromagnetic waves emitted by the molecule motion of receptor objects and show similar amplitude of vibration to the electromagnetic waves emitted by the molecule motion of receptor objects (the amplitude of vibration between these two waves should not show large variation), is able to accelerate the revolution/rotation motion of receptor molecules (or atoms) most effectively [11]." Consequently, it is concluded that the occurrence probability in 'quantum superposition' state among different elementary particle waves determines the efficiency of interactions among different sources of elementary particle waves. The higher occurrence probability in 'quantum superposition' state, the higher efficiency in quantum wave interactions. However, this efficiency in quantum wave interaction has not been integrated into quantum wave function so far, consequently becoming the research gaps in future study.

With regards to the effects of incident angle on the diffraction pattern (Figure 12), the case study explains that if the crystal displays more regular lattice arrangement, which also means higher symmetry among adjacent lattices, the changed incident angles may lead to less influences on the intensity of diffraction points [40]. However, in addition to the structural regularity among different lattices, my article further argues that the symmetry of magnetic line structure within a lattice of crystal also significantly influences the diffraction pattern, because my another article has previously proposed that the diffraction of light wave is caused by the interaction between the magnetic field on the obstacle surface and the polarity of light wave [10]. Consequently, the higher symmetry of magnetic line structure within a unit of lattice results in less effects of incident angles on the intensity of diffraction points.

Figure 11 tests the effect of sample thickness on the diffraction patterns, which may be attributed to the regularity of lattice's space arrangement: the more regular and uniform space arrangement among different crystal lattices, the less effect caused by changing sample thickness. Consequently, compared with crystal orientation [-111], the sample of crystal orientation [011] would display more regular and uniform space arrangement among lattices, so its diffraction pattern does not apparently vary with the increased sample thickness for [011] crystal orientation, whereas the diffraction pattern significantly is changed by the increased sample thickness for [-111] crystal orientation. Consequently, measuring the effect of different sample thickness on the diffraction pattern by using equipment can be used to test the regularity of lattice's space arrangement for different crystal orientations, which may become the newly proposed method in my article.

My another article demonstrates 'dark matter' from the prospective of Van der Waals force formation, which is defined as the energy binder polymerizing elementary particles to form aggregate and this energy binder underlies in the fourth dimensional

spaces. The characteristics of this 'dark matter' is to generate the non-linear buffer force against the external destructive force; and the adhesion force generated by this energy binder function of 'dark matter' is usually reduced by decreasing the materials temperature [4]. Consequently, 'dark matter' shows 'plasticity' characteristics in materials, and this article tries to analyze the findings of above case studies according to my new definition of 'dark matter': firstly, the temperature of spectral materials needs to be adjusted into the suitable degenerate temperature so that both signal and idler waves' center wavelengths can be coincided at the same level. The temperature variation alters the adhesion force generated by the energy binder of 'dark matter', which further influences the cutting motion of elementary particles against the fourth dimensional magnetic line (the cutting motion direction is indicated by the red arrow in Figure 2), so the frequency of electromagnetic waves produced by the cutting motion of elementary particles is correspondingly changed; Next, it is to further explore the formation mechanism of both diffraction and refringence of elementary particle waves (shown in Figure 13): when a beam of elementary particles collides with the atoms or lattices of obstacle object materials (the transmission direction of elementary particle wave is indicated by the blue arrow in Figure 13), the shielding effect of the electric field inside the atom or lattice stops the elementary particle waves from penetrating through the atom or lattice, so the beam of elementary particles is forced to transmit on the surface of the atom or lattice. The 'plasticity' characteristics of dark matter underlying elementary particle waves results in the polarization under this condition, which generates asymmetric distribution between wave peak and bottom along the transmission direction of elementary particle wave (wave peak is not located at the middle of half wave in Figure 13). This polarization of elementary particle waves may easily alter the frequency and intensity of diffraction or refracted waves, because the adhering force of dark matter is changed by the asymmetric alteration.

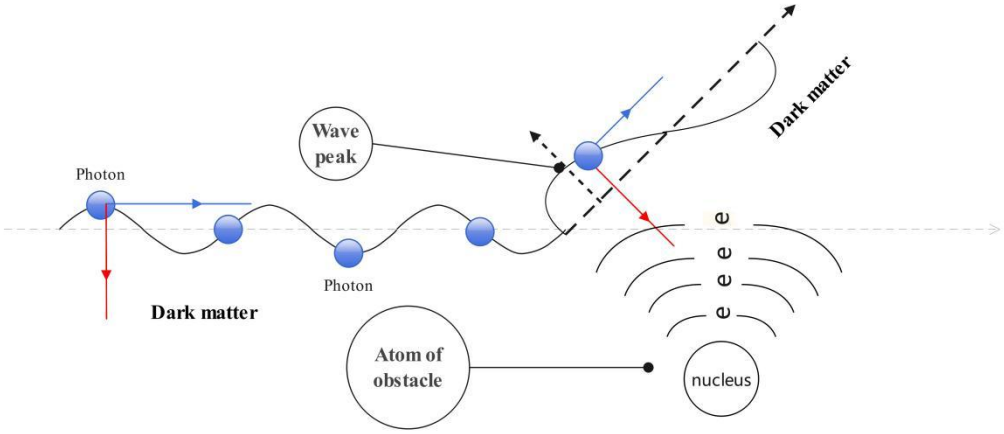



**Figure 13. Polarization of elementary particle waves.**

In 4.6 section of this article, the example of double-slit experiment does not take the polarization of elementary particle waves into consideration, when it is used to

illustrate the diffraction mechanism of quantum wave. Similarly, in Figure 7 and Figure 8, when the intensity value is not included in diffraction modeling, the intensity is evenly distributed in each diffraction point. However, when the intensity value is simulated in diffraction modeling, the intensity varies significantly among different diffraction points, which can be attributed to the polarization formation of elementary particle waves discussed in Figure 13.

In 4.5 section of this article, Bohr atomic quantum model is established to quantify the hydrogen atomic spectrum [19]. Based on the theory of atomic spectral analysis, the electrons at the lower energy orbitals absorb light waves at specific wavelength ranges, turning into excited state, and then are transitioned to higher energy orbitals [38]. This article designs a new model of De Broglie wave according to Bohr atomic quantum model and hydrogen spectral analysis (Figure 14):

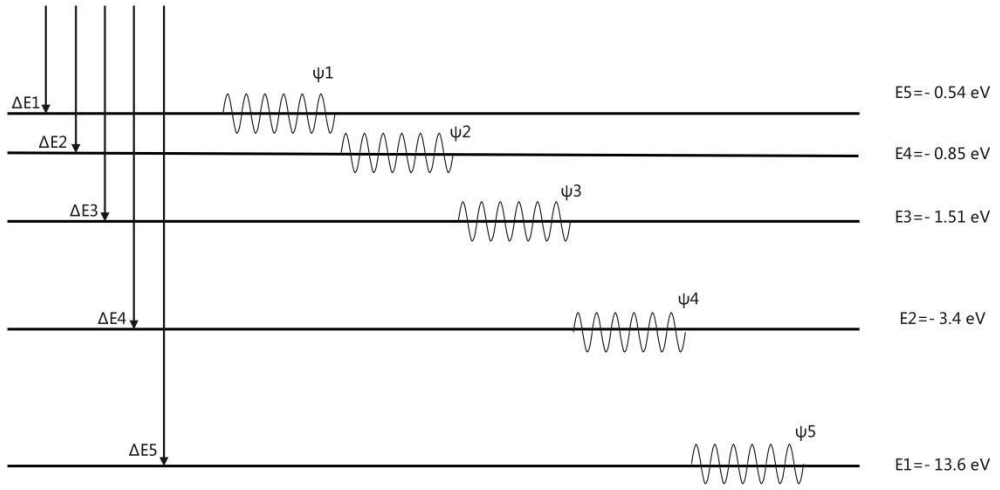



**Figure 14. Conceptional model of De Broglie wave in the electron orbital transition process in hydrogen atom.**

Figure 14 describes the conception model of De Broglie wave in the electron orbital transition process according to the hydrogen spectrum. For example, when the electron stays at the energy orbital of E5 (- 0.54 eV), its Schrodinger wave equation is expressed as ψ1. Then the electron absorbs external energy of ΔE2, and it is transitioned to higher energy orbital of E4 (- 0.85 eV), so the Schrodinger wave equation is re-expressed as ψ2. There are mainly two reasons to explain that the linear superposition of wave functions is NOT applicable on this new conception model: firstly, the wave motion becomes the math mode of 'jumping points' when the electrons transfer between different energy orbitals, and the differential and integral calculus in maths can not be implemented in this process; secondly, at different energy orbitals, the frequency of free particle wave is significantly different, which means that it is NOT under the 'quantum superposition' state defined in the section

4.9 of this article so that the superposition of different wave functions is meaningless. As discussed above, only when two elementary particle waves' frequencies coincide at the same level, interference in two waves occurs so that the 'quantum superposition' can become applicable. Consequently, a new math model of piecewise function is designed below to express the De Broglie wave, taking the factor of electron orbital transition process into consideration:

$$\begin{cases} \psi a(r,t) = A \times \exp[\frac{i}{\hbar} \times (p \times r - Ea \times t)] & \text{Energy orbital} = E1 \\ \psi b(r,t) = A \times \exp[\frac{i}{\hbar} \times (p \times r - Eb \times t)] & \text{Energy orbital} = E2 \\ \psi c(r,t) = A \times \exp[\frac{i}{\hbar} \times (p \times r - Ec \times t)] & \text{Energy orbital} = E3 \end{cases}$$

$$\text{.....} \qquad \text{.....} \qquad \text{.....}$$

$$\psi x(r,t) = A \times \exp[\frac{i}{\hbar} \times (p \times r - Ex \times t)] \qquad \text{Energy orbital} = En$$

Equation 70

In this equation 70, the value range of X is (a,b,c,.....,x), representing the symbol of different substance plane wave functions ($\psi_a(r,t)$, $\psi_b(r,t)$, $\psi_c(r,t)$,...,$\psi_x(r,t)$) corresponding to each electron energy orbital (E1, E2, E3,.....En); Variables of Ea, Eb, Ec, ..... Ex represent the kinetic energy of free particles at each energy orbital; E1, E2, E3,..... En represent different energy orbitals; The other variables of equation 70 have been described in equation 52 and above section 4.3 of this article. Setting up three different energy orbitals (E1, E2 or E3) as the example in equation 70, at each energy orbital, the free particle plane wave function is still valid with constant kinetic energy value of Ea, Eb and Ec respectively (constant kinetic energy value of Ea, Eb and Ec can be calculated as the mean value at each energy orbital respectively), but different wave functions of free particle can not be the linear superposition among different energy orbitals. The whole piecewise function's philosophy reflects the conclusion of experiment results in section 8.3, which reports that both particle energy and momentum are NOT constant in particle collision experiment. At each energy orbital (E1, E2, E3,.....En), the corresponding substance plane wave function ($\psi_a(r,t)$, $\psi_b(r,t)$, $\psi_c(r,t)$,...,$\psi_x(r,t)$) can still go through the same deducing steps that have been described in section 5 (from equation 52 to equation 66), and each Schrodinger wave equation is finally derived for different energy orbital. Then this improved Schrodinger wave equation would be more appropriate to simulate the density of electron clouds inside an atom in 3D modeling of quantum chemistry, which will be further implemented in the next modeling section of this article. Of course, equation 70 is also applicable on other elementary particle waves (such as protons), because it is believed that the protons' rotation orbitals inside the nucleus are also differentiated by different energy orbitals, and 4.7 section of my article has explained that De Broglie wave equation covers the wave-particle duality of all the microscopic particles.

It is further concluded that the variation in both particle energy and momentum for a specific type of elementary particle, as reported by particle collision experiment results in section 8.3 of this article, is mainly caused by two reasons: the elementary particle mass varies in the three-dimensional spaces during the wave-like transmission motion (shown in Figure 4); secondly, the charged elementary particles' states may differ in the acceleration process of particle collision experiment, because these charged elementary particles may be still under different energy orbitals in the particle acceleration process.

Figure 6 divides the De Broglie wave into mass wave and energy wave (both electric and magnetic field energy), so the calculation equations should be different for each type correspondingly. The above piecewise function (equation 70) based on free particle plane wave function should be more applicable on the mass wave calculation; For the energy wave under diffraction or reflected conditions, it is to take the theory of 'Black Body' radiation and absorption into consideration, which is discussed in 3.2 section of this article, and the equation is expressed as:

Diffraction condition: $E_{\text{incident wave}} = E_{\text{diffraction wave}} + E_{\text{absorption by blackbody}}$

Equation 71

or

Reflection condition: $E_{\text{incident wave}} = E_{\text{reflected wave}} + E_{\text{refracting wave}} + E_{\text{absorption by blackbody}}$

Equation 72

$E_{\text{electromagnetic wave}} = \sum_0^{\lambda} f(\lambda)$ and Intensity = $f(\lambda)$

Equation 73

or $E_{\text{electromagnetic wave}} = \int_0^{\lambda} f(\lambda)$

Equation 74

In equation 71, the electromagnetic energy of incident wave ($E_{\text{incident wave}}$) is divided into electromagnetic energy of diffraction wave ($E_{\text{diffraction wave}}$) and electromagnetic energy absorbed by blackbody ($E_{\text{absorption by blackbody}}$) under diffraction conditions; equation 72 reveals that the electromagnetic energy of incident wave ($E_{\text{incident wave}}$) is the sum of electromagnetic energy of reflected wave ($E_{\text{reflected wave}}$), electromagnetic energy of refracting wave ($E_{\text{refracting wave}}$), and electromagnetic energy absorbed by blackbody ($E_{\text{absorption by blackbody}}$) under reflection conditions; equation 73 demonstrates that the electromagnetic energy of electromagnetic wave ($E_{\text{electromagnetic wave}}$) is the total sum of electromagnetic intensity value ($Intensity = f(\lambda)$) at each wavelength ($\lambda$); if the equipment's outputting results is expressed as the linear function, then equation 74 is applicable on calculating the total sum of electromagnetic intensity value ($f(\lambda)$) at each wavelength ($\lambda$).

It is worthwhile mentioning that the equipments used to measure the kinetic energy in equation 70 and to measure the electromagnetic energy in equation 71 ~ equation 73 are different. The method to measure the kinetic energy of free particles in equation

70 has been introduced in section 4.2, and the electromagnetic energy of free particles can be measured by electromagnetic wave detector, a common equipment used. Consequently, the above equations are not only the conceptional models for better understanding, but also become the feasible solution in measuring practice.

Previous case study chosen by this article has reported that the experiment results by using interferometers are inconsistent with the theoretical equation calculation [39], and Figure 7 ~ Figure 10 of this article also show that the theoretical motion modeling results are also sometimes not consistent with the empirical dynamics modeling results of diffraction pattern. The new conceptional functions (equation 70 ~ equation 73) designed in my article may achieve more consistency and reduce the uncertainty in the modeling of De Broglie wave.

## 10.Three-Dimensional modeling of quantum chemistry

My previous article's plan used to design a time-dependent and one-dimensional matrix to simulate the chemistry reaction rate by selecting NetLogo software to edit, but C++ Language was subsequently chosen to edit instead of NetLogo [42]. To better fit the model, the three-dimensional arrays are adopted to simulate the 3-dimensional space, instead of previous time-dependent and one-dimensional matrix:

To enter the initial values of the decimal variables (0.00): Density1 and Density2, and the decimal variables of both Density1 and Density2 are estimated according to the concentrations of chemical reactant species 1 (molecule 1) and chemical reactant species 2 (molecule 2) in the three-dimensional space simulated in this program, respectively [42];

To enter the values of integer variables I, J, K, and the integer variables of I, J, K represent the total spatial grid amount at x, y, z axis of the three-dimensional space respectively simulated in this program;

To enter the values of integer variable T, and the integer variable of T represents the total time intervals simulated in this program;

To enter the values of the decimal variables: P1 and P2, and the decimal variables of both P1 and P2 refer to the proportion of the specific spherical surface area of active chemistry bonds in molecule 1 and molecule 2 respectively, to its whole spherical surface area of a molecule during the molecular revolution. The philosophy of simulating variables P1and P2 is discussed in my article [42];

The calculation steps during the cycle of the first time interval include:
To set the three-dimensional array: a[i][j][k] (i<=I; j<=J; k<=K), where i, j, k is the spatial grid number at x, y, z axis respectively, and it is to choose a number of "0" or "1" as each value of a[i][j][k]. The probability of choosing the number "1" is a linear

function of P1 * Density1. Each value of a[i][j][k] represents the occurrence of molecule 1 in a spatial grid at the coordinate point (i,j,k). If molecule 1 occurs in a spatial grid, its value is given to be 1; otherwise its value is given to be 0;

To set the three-dimensional array: b[i][j][k] (i<=I; j<=J; k<=K), where i, j, k is the spatial grid number at x, y, z axis respectively, and it is to choose a number of "0" or "1" as each value of b[i][j][k]. The probability of choosing the number "1" is a linear function of P2 * Density2. Each value of b[i][j][k] represents the occurrence of molecule 2 in a spatial grid at the coordinate point (i,j,k). If molecule 2 occurs in a spatial grid, its value is given to be 1; otherwise its value is given to be 0;

Setting the three-dimensional array: c[i][j][k] (i<=I; j<=J; k<=K), where i, j, k is the spatial grid number at x, y, z axis respectively, and the value of the three-dimensional array c[i][j][k] is calculated as the three-dimensional array a[i][j][k] multiplied by the three-dimensional array b[i][j][k]; c[i][j][k] represents the interaction between molecule 1 and molecule 2;

To set the variable of 'Reaction', which refers to the total amount of "1" value in the three-dimensional array c[i][j][k], representing the total amount of spatial grids in which the chemistry reaction occurs. The value of variable 'Reaction' represents the amount of chemistry reaction product;

Then the value of Density1 turns to be the initial value minus "E*Reaction"; the value of Density2 turns to be the initial value minus "F*Reaction". This step shows that the concentration of chemical reactants (molecule 1 and molecule 2) will be reduced correspondingly due to the chemistry reaction. However, both Density1 and Density2 cannot be less than 0 in this simulation process. The constants of E and F are assumed as value 0.005 and 0.003 respectively for modeling test purpose in this program;

To repeat the cycle of the second time interval until the "T" times cycle of time interval.

After the "T" times cycle of time interval, it is to output the the three-dimensional array of c[i][j][k], the total sum value of variable 'Reaction' from the first time interval to the "T" time interval, the updated value of both 'Density1' and 'Density2'.

Finally the total sum value of variable 'Reaction' can be converted into the concentration of chemistry reaction product generated during the total chemistry reaction cycle, and the updated concentrations of chemical reactants (molecule 1 and molecule 2) can be also derived after the "T" times cycle of time interval. This three-dimensional numerical model reflects the philosophy of [0,1] binary algorithm in nature, which has been substantially discussed in my article [42]. The advantage of three-dimensional array adopted in this model will better fit the three-dimensional space simulation, which facilitates other sub-models to integrate, including the

diffusion models (such as Gaussian diffusion model) and the 3D model of boundary layer formation designed in my another research [30]. In addition, the test of sensitivity analysis for each parameter (such as constants of E=0.005 and F=0.003 assumed in this program) must be conducted before application, which has been illustrated by my another numerical modeling article [43].

Modeling test is conducted next: the initial Density1 and Density2 are assumed as 10.00 and 9.00 respectively; P1 and P2 are assumed as 0.05 and 0.06 respectively; and it is to test the modeling results from time interval 1 to time interval 20.

The source codes (Dev-C++ 6.5 Version):

```
//All rights reserved by Liu Huan; Source from:https://doi.org/10.58473/JQPMC0014

#include <iostream>
#include <random>
#include <vector>
#include <iomanip>
#include <algorithm>

using namespace std;

const double E=0.005, F=0.003;
vector<vector<vector<int>>> generateArray(int I, int J, int K, double probability) {
	random_device rd;
	mt19937 gen(rd());
	uniform_real_distribution<> dis(0.0, 1.0);

	vector<vector<vector<int>>> arr(I, vector<vector<int>>(J, vector<int>(K)));
	for (int i = 0; i < I; i++) {
		for (int j = 0; j < J; j++) {
			for (int k = 0; k < K; k++) {
				arr[i][j][k] = (dis(gen) < probability) ? 1 : 0;
			}
		}
	}
	return arr;
}

int countOnes(const vector<vector<vector<int>>>& arr) {
	int count = 0;
	for (const auto& layer : arr) {
		for (const auto& row : layer) {
			for (int val : row) {
```

```
                    if (val == 1) count++;
                }
            }
        }
        return count;
}

void printArray(const vector<vector<vector<int>>>& arr) {
        for (int i = 0; i < arr.size(); i++) {
            cout << "Layer " << i << ":" << endl;
            for (int j = 0; j < arr[0].size(); j++) {
                for (int k = 0; k < arr[0][0].size(); k++) {
                    cout << arr[i][j][k] << " ";
                }
                cout << endl;
            }
            cout << endl;
        }
}

int main() {
        double Density1, Density2, P1, P2;
        int I, J, K, T;

        cout << "To input the decimal values (0.00) of Density1 and Density2 (leaving a
space in the middle): ";
        cin >> Density1 >> Density2;
        cout << "To input the integral values of I, J, K (leaving a space among values): ";
        cin >> I >> J >> K;
        cout << "To input the time intervals T: ";
        cin >> T;
        cout << "To input the value of P1 and P2 (leaving a space in the middle): ";
        cin >> P1 >> P2;

        vector<vector<vector<int>>> final_c;
        int total_Reaction = 0;
        double final_Density1 = Density1, final_Density2 = Density2;

        for (int iter = 0; iter < T; iter++) {
            auto a = generateArray(I, J, K, P1 * Density1);
            auto b = generateArray(I, J, K, P2 * Density2);

            vector<vector<vector<int>>> c(I, vector<vector<int>>(J, vector<int>(K)));
            for (int i = 0; i < I; i++) {
```

```
                for (int j = 0; j < J; j++) {
                    for (int k = 0; k < K; k++) {
                        c[i][j][k] = a[i][j][k] * b[i][j][k];
                    }
                }
            }

            int Reaction = countOnes(c);
            total_Reaction += Reaction;
            Density1 = std::max(0.0, Density1 - E * Reaction);
            Density2 = std::max(0.0, Density2 - F * Reaction);

            if (iter == T - 1) {
                final_c = c;
                final_Density1 = Density1;
                final_Density2 = Density2;
            }
        }

        cout << "\nThe " << T << " Times cycle:" << endl;
        cout << "c[i][j][k]:" << endl;
        printArray(final_c);
        cout << "Total products (from the first time interval to the " << T << " times time
interval): " << total_Reaction << endl;
        cout << "Updated Density1: " << fixed << setprecision(2) << final_Density1 <<
endl;
        cout << "Updated Density2: " << fixed << setprecision(2) << final_Density2 <<
endl;

        return 0;
}
```

Acknowledgement in this section: the basic functions of computing source codes are looked up by using Deepseek models, and Copilot gives the advice to improve the model.

## 11.Conclusion

This observational study has revealed the generation mechanism of electric charges carried by the elementary particles, and explored the generation of electromagnetic wave by the wave-like transmitting movement of photons in dark matter, based on which the relationship among mass, energy and momentum is re-built by presenting the new math equations. The ‘Blackbody’ theory is re-explained by the shielding

effects of equipotential lines inside an atom. The De Broglie wave of elementary particles (such as protons, electrons or photons) is clarified and classified into mass wave and energy wave. Some basic conceptions of quantum physics are clarified and re-defined by this article. The classical physics relationship among mass, energy and momentum is re-analyzed on the basis of elementary particle collision data in response to the newly proposed equations in this article. The spectral materials' characteristics are re-analyzed according to the spectral interferometer's measuring data and transmission electron microscopy's modeling data. Finally a three-dimensional modeling is edited to simulate the quantum chemistry reaction process as the AI & Applied Maths programmer.

关键知识点译文：

1.机械运动亦称为力学运动，指代物质的质点在时间、空间中的位移矢量变化，区别于仅仅以能量物质存在的运动。本文根据本人在另一篇量子物理学论文中对于光子的新定义[13]，将光子作为机械运动的最基本的研究对象，也是质量物质中最微小的质点分割单元，因此电磁波的波粒二象性定理是质量物质的一种基本属性，并非局限于能量物质的基本属性。

2.根据本人一篇论文中的图 1 [11]，进一步论述原子内部电场屏蔽效应与电子轨道的论点：对于同一种元素的相邻原子，产生的电磁波频率相同，因此相邻原子之间很容易形成电磁波的干涉波；相长干涉与相消干涉区域之间，形成多条等位线（等势线）。相消干涉区域由于波峰与波谷相抵，相对中性，电子会倾向于在相消干涉区域做自转运动，从而成为影响电子自转轨道的重要因子。在图 1 这种运动模型中，原子内部的电场屏蔽作用使得电子轨道一定相对固定，并非无序随机型；电子倾向于在某一条闭合环形等位线的外层空间做自转运动，符合电场屏蔽作用的形成条件。

3.与原子内部电场屏蔽效应进行对比与对照，宏观天体（比如恒星与行星）的星球内部也一定存在场量屏蔽效应，但是与微观原子内部的屏蔽效应不同，宏观天体主要依靠物质边界层形成场量屏蔽效应。边界层破裂导致屏蔽效应的破坏，这是导致各种自然灾害（比如龙卷风、地震、太阳耀斑等[6][7][8]）的主要因素，因此稳定的边界层以及产生的场量屏蔽效应是天体演化运动中重要影响因子。与微观原子内部等位线相似，天体内部的整体等位线一定倾向于闭合环形，由于等位线产生的屏蔽效应，物质沿着等位线两边做平行运动[12]。这种运动规律是我们所在的三维空间中的天体能够演变成为有规则球体形状的主要因素。

4.在假设德布罗意波分为质量波和电磁能波的前提下，德布罗意波的波粒二象性可以很容易被理解：德布罗意波不仅具备经典物质波的质量粒子属性，还在量子水平上表现出由基本粒子束（光子、电子、质子等）生成并携带的电磁能波的物理量。因此，接下来需要分别计算德布罗意波的质量波和电磁能波的波函数。在新的定义中，虚数概念指代在量子波中基本粒子的相位，具备现实、实际的物理性质，并非一种仅仅为了简化数学运算而引入的数学技巧。

4. 总之，本文首先回顾经典力学原理，这些经典力学原理都在一个共同的局限条件下可以有效解决物理学上实际问题，即：宏观物理条件和低速运动模型。在量子微观尺度、跨星系运动模型、物质材料衰老等情境下，新的物理学模型需要建立起来才能解决实际问题。本人之前的论文已经充分论述了微观量子领域中粒子对撞运动模型[1]、原子整体结构的电场屏蔽作用下微观量子力学模型[10]、原子内各质点的受力平衡分析[2][3]、分子间作用力起源 [4]、材料在衰老过程中的热运动模型[5][9]、摩擦阻力的量子模型[4]、游离与自由态带电粒子在自然界物质边界层中的运动模型[6][7]、暗物质原理在跨星系间运动模型中的应用[8]等等。因此本文在表格 2 中全面总结了本人在之前论文以及本篇论文中论述的原创型力学模型。

## References:

[1]. Liu Huan. (2021). Quantum Mechanics. Journal of Environment and Health Science (ISSN 2314-1628), 2021(02). https://doi.org/10.58473/JQPMC0001
[2]. Liu Huan. (2022). Essay: Electromagnetics and Materials. Journal of Environment and Health Science (ISSN 2314-1628), 2022(11). https://doi.org/10.58473/JQPMC0004
[3]. Liu Huan. (2021). The anti-matter of symmetric three-dimensional spaces along the fourth dimension axis. Journal of Environment and Health Science (ISSN 2314-1628), 2021(2). https://doi.org/10.58473/JAES0002
[4]. Liu Huan. (2021). Van der Waals force and Dark Matter. Journal of Environment and Health Science (ISSN 2314-1628), 2021(02). https://doi.org/10.58473/JQPMC0006
[5]. Liu Huan (2021). The Principal of Thermodynamics: The Inner Energy, Energy Loss and Materials Perishing /热力学原理：内能，能量损耗与材料老化. 2021 (02). Journal of Environment and Health Science. https://doi.org/10.58473/JQPMC0008
[6]. Liu Huan. (2021). Discussion of Tornado Formation Mechanism. Journal of Environment and Health Science (ISSN 2314-1628), 2021(08). https://doi.org/10.58473/JAES0007
[7]. Liu Huan. (2021). The formation mechanism and forecasting of earthquakes. Journal of Environment and Health Science (ISSN 2314-1628), 2021(09). https://doi.org/10.58473/JAES0008
[8]. Liu Huan. (2023). Essay: original review of high-dimensional spaces and astronomy theories in modern physics. Journal of Astronomy and Earth Sciences (ISSN2958-4043). 2023 (07). https://doi.org/10.58473/JAES0010
[9]. Liu Huan. (2021). Essay: Materials and Thermodynamics. Journal of Environment and Health Science (ISSN 2314-1628), 2021(11). https://doi.org/10.58473/JAES0012
[10]. Liu Huan. (2021). Molecular Attributes of 'Revolution' Motion in Materials. Journal of Environment and Health Science (ISSN 2314-1628). https://doi.org/10.58473/JQPMC0007
[11]. Liu Huan. (2021).The Principal of Thermodynamics: Specific Heat Capacity and Material. Journal of Environment and Health Science (ISSN 2314-1628), 2021(02). https://doi.org/10.58473/JQPMC0009
[12]. Liu Huan. (2021). The formation mechanism of substance boundary layers. Journal of Environment and Health Science (ISSN 2314-1628), 2021(2). https://doi.org/10.58473/JAES0004
[13]. Liu Huan. (2021, Latest revised on 2025-02-24b). Essay: Quantum and Materials. Journal of Environment and Health Science (ISSN 2314-1628), 2021(12). https://doi.org/10.58473/JQPMC0003
[14]. 力学。搜狗百科。
[15]. 光子。搜狗百科。
[16]. 质能方程。搜狗百科。
[17]. Liu Huan. (2021). The particle dualism of electromagnetic waves. Journal of

Environment and Health Science (ISSN 2314-1628), 2021(2). https://doi.org/10.58473/JQPMC0002
[18]. Liu Huan. (2021). The magnetism across time-spaces and the driving force of celestial rotation. Journal of Environment and Health Science (ISSN 2314-1628), 2021(2). https://doi.org/10.58473/JAES0003
[19]. 陈小华,袁定旺,刘智骁.工程量子力学[M].化学工业出版社:202311.212.
[20].黑体辐射。搜狗百科。
[21].物质波。搜狗百科。
[22].巴尔末公式。搜狗百科。
[23].薛定谔方程。搜狗百科。
[24].牛顿第一定律。搜狗百科。
[25].牛顿第二定律。搜狗百科。
[26].牛顿第三定律。搜狗百科。
[27].万有引力定律。搜狗百科。
[28].经典力学。搜狗百科。
[29].魏岗,关晖.流体力学基础与应用[M].气象出版社:201801.288.
[30].Liu Huan (2024). Exploring the formation of ocean current and the underlying hydrology. Journal of Astronomy and Earth Sciences (ISSN2958-4043). 2024 (12). https://doi.org/10.58473/JAES0011
[31].Liu Huan. (2021). Electricity and Stability of Electron orbits in Atom. Journal of Environment and Health Science (ISSN 2314-1628), 2021(02). https://doi.org/10.58473/JQPMC0005
[32]. 孙艳坤. 北京谱仪III上 e~+e~-→Φη'，ΦK~+K~-和 K~+K~-K~+K~-过程中共振结构的寻找[D].中国科学技术大学,2019. DOI:10.27517/d.cnki.gzkju.2019.000218.
[33]. 班正灵. 北京谱仪III上ψ(2S)→π~03(π~+π~-)和 J/ψ→γ3(π~+π~)的实验研究[D].广西师范大学,2020.DOI:10.27036/d.cnki.ggxsu.2020.001036.
[34]. 潘祥. 北京谱仪III实验上 D~+→ηπ~0π~+，D~+→ηηπ~+和 D~0→ηπ~-π~+衰变绝对分支比测量[D].苏州大学,2019.DOI:10.27351/d.cnki.gszhu.2019.001597.
[35]. 张宏宏. 北京谱仪III实验上ψ(3686)→Λ(?)ω和 J/ψ→Λ(?)η的研究[D].广西师范大学,2019.
[36]. 张宏宏.在北京谱仪实验上ψ（3686）→Λ(?)ω和 J/ψ→Λ(?)η的研究[D].吉林大学,2024.DOI:10.27162/d.cnki.gjlin.2024.000866.
[37]. 伍雄浩. 北京谱仪上 τ→3Kντ 分支比上限的测量[D]. 吉林大学,2024.DOI:10.27162/d.cnki.gjlin.2024.003476.
[38].Liu Huan (2023). Original review of quantum chemistry and 3D modeling of artificial intelligence. Journal of Quantum Physics and Materials Chemistry (ISSN2958-4027). 2023 (11). https://doi.org/10.58473/JQPMC0013
[39]. 曾梓琦. 量子干涉仪的实验与理论研究[D]. 武汉工程大学,2024.DOI:10.27727/d.cnki.gwhxc.2024.000049.
[40]. 程珑.动力学方法与量子轨迹方法研究电子在晶体中的衍射及成像[D].中国科学技术大学,2021.DOI:10.27517/d.cnki.gzkju.2021.000141.
[41].弹性散射与非弹性散射。搜狗百科。
[42].Liu Huan. (2021). Ancient Chinese Eight Diagrams and Application on

Chemistry Reaction Rate. Journal of Environment and Health Science (ISSN 2314-1628), 2021(02). https://doi.org/10.58473/JQPMC0010
[43].Liu Huan (2021). Modeling of annual net primary production of a forest in the Taramakau Valley, Westland, New Zealand. Journal of Environment and Health Science (ISSN 2314-1628). 2021 (02). https://doi.org/10.58473/JEHS0007